The role of visuomotor coupling in the development of sensory processing in mouse visual cortex

Inauguraldissertation

zur

Erlangung der Würde eines Doktors der Philosophie

vorgelegt der

Philosophisch-Naturwissenschaftlichen Fakultät

der Universität Basel

von

Bo Wang

von Volksrepublik China

Basel, 2017

Genehmigt von der Philosophisch-Naturwissenschaftlichen Fakultät
auf Antrag von

Prof. Dr. Thomas Mrsic-Flogel

Dr. Georg Keller

Prof. Dr. Richard Hahnloser

Basel, 21.03.2017

Prof. Dr. Martin Spiess

The Dean of Faculty

Table of contents

Abstract 4

Introduction 5

Representation framework 5

Predictive coding framework 5

Visuomotor coupling 6

Motor-related signals in V1 7

Results 9

Responses in excitatory neurons 10

Responses in inhibitory neurons 11

Response change in the time course 14

Behavior 15

Gene expression 16

Discussion 17

Figures and tables 20

Methods 43

Acknowledgements 50

References 51

Abstract

The current prevailing understanding of sensory processing in cortical areas is largely based on the presentation framework proposes that neural activity form presentations of external stimulus. However, with recent advances in technologies of recording neuronal activity in awake behaving animals, it has been shown that the primary visual cortex (V1) is also strongly driven by self-movement, suggesting that the presentation framework of visual cortex function is incomplete. Particularly, a subset of neurons in V1 selectively respond to transient visuomotor mismatches, and it could be explained by the predictive coding framework which postulates V1 compares the predicted and received visual input and sense the difference between the two. Experience of normal visuomotor coupling has been shown to be crucial for the development of visual-guided behavior, therefore it is likely that the prediction of visual input depends on the experience of visuomotor coupling, which shapes the functional development of V1.

In the present study, we use a virtual reality system and trained dark-reared mice with either normal or random visuomotor coupling, and recorded the neural activity in layer 2/3 neurons of V1. We show that mismatch responses in excitatory neurons were strongly dependent on visuomotor experience. By recording several different types of layer 2/3 interneurons in V1 and manipulating their activity with designer receptor exclusively activated by designer drugs (DREADDs) or optogenetics tools, we propose a circuit model showing that the mismatch response could be the result of a disinhibition mediated by local somatostatin (SST) interneurons. Mismatch responses in both groups of mice with different visuomotor training conditions merged together after they were transferred to normal rearing environment. These data demonstrate that neurons in layer 2/3 mouse V1 computes a difference between an excitatory motor-related input and an inhibitory visual input, where the balance between the two inputs is finely tuned by visuomotor experience.

Introduction

Vision provides a major fraction of the information we receive, process, and perceive in our everyday life. Thus, the visual system, the part of our nervous system which takes charge of vision, plays a pivotal role in our interaction with the environment. In mammals, visual processing starts when light hits on the retina, where light is transformed into neural signals and are sent to a part of thalamus called lateral geniculate nucleus (LGN); from there the signals are further relayed to primary visual cortex (V1), which is the main brain area focused in this thesis.

Representation framework

The representation framework of visual cortex function is the idea that neural activity in the visual cortex serve to form a representation of external stimuli (Marr, 2010). This framework is largely based on the concept of receptive field and is currently the prevalent understanding of visual cortex function.

The term “receptive field” was coined in 1906 by neurophysiologist Sir Charles Scott Sherrington in the somatosensory context (Sherrington, 1906), and was adapted in the sense of single neurons in the visual system by Hartline (Hartline, 1938). Horace Barlow later discovered inhibitory surround in the receptive field in frog’s retina, provided the first evidence for “feature detector” hypothesis, as described in the paper: “It is difficult to avoid the conclusion that the 'on-off' units are matched to the stimulus and act as fly detectors (Barlow, 1953).” Many related studies on receptive field followed (Spillmann, 2014), including works by Hubel and Wiesel who showed elongated-shape-receptive fields with selective orientations and positions. Hubel and Wiesel termed “simple”, “complex” and “hypercomplex” cells based on the receptive field properties of the neurons they recorded (Hubel and Wiesel, 1962, 1959). Follow the notion of the above findings, David Marr summarized in his book using the term “representational framework” suggesting that the function of the visual system is to form a representation of the external stimuli, i.e. light intensities. This representation has multiple hierarchical levels, with lower levels form relatively simple features such as edges and bars, feedforward to higher levels where signals integrated to form more complex features and ultimately a perception of a 3D object (Marr, 2010).

Predictive coding framework

Visual signals in the natural world are highly redundant. It is of general interest of signal transmission to reduce this redundancy for better efficiency. Horace Barlow suggested that sensory neurons encode a representation of sensory stimuli based on its statistical characteristics to save the limited bandwidth of the sensory processing pathway, as called efficient coding hypothesis (Barlow, 1961).

As an extension of this, there has been an increasing number of theoretical works on the predictive coding strategy of the brain.

Rao and Ballard proposed a predictive coding model of visual processing in the cortex. In their model, the visual system consists of multiple processing levels, just like in the presentation hypothesis. The key difference here is that the model make use of top-down signals as predictions of the incoming signal received in the adjacent lower level. At each level, the difference between the received and predicted signal is calculated, and only this difference (referred to as "residual error") is propagated further to the higher level. In this way, as Rao and Ballard suggested, the dynamic range of coding capacity of the visual system is more efficiently used (Rao and Ballard, 1999). Spratling also suggested a modified version based on Rao and Ballard's model (Spratling, 2008). Notably, Friston provided a unified predictive coding framework under the free energy principle (Friston and Kiebel, 2009). Also see (Clark, 2013) for a more comprehensive review on predictive coding.

The predictive coding framework is a step forward over the representation framework. In addition to the classical feedforward bottom-up signals, the feedback top-down signals are arguably equally important, and a function of sensory cortex is to compare the two and compute the difference. This way of understanding could even be applied to the function of cortex or even the brain in general.

Visuomotor coupling

Sensory feedback is inherently coupled to movement, as in the case of vision, we see a flow of change in our visual field as a result of our own movements. The importance of visuomotor coupling was first revealed by pioneering visual neuroscience studies. Early experiments have shown that kittens reared in a holder with exposure to a patterned environment failed at a movement discrimination task, while kittens reared with free moving in the same environment appeared normal as control groups (Riesen and Aarons, 1959). This suggests that visuomotor coupling is required for the development of functional vision. Interestingly, similar observations were also made in several human studies, in which subjects were asked to wear wedge prisms in front of their eyes. Subjects were able to quickly adapt to the rearranged visual coordinates, and this adaptation only happened when voluntary bodily movements were involved (Held and Bossom, 1961; Held and Freedman, 1963).

This notion is further demonstrated by Held and Hein with an elegantly designed experiment. In this classic experiment, they reared kittens in complete darkness from birth, and started training them in a custom-built apparatus, referred to as a "kitten carousel". Of the two kittens being trained simultaneously, only one of them had its paws on the floor of the apparatus, thus being able to control the rotation of the whole apparatus (referred to as the active kitten), while the other kitten

had no influence on the rotation when it moves (referred to as the passive kitten). In this way, only the active kitten has the visual feedback coupled with its own movements (Held and Hein, 1963). The beauty of this design is that the visual stimulus received by the pair of kittens is well controlled, as provided by the vertical gratings painted on the wall, and both kittens can freely move during the exposure to the apparatus. Thus, the only difference between the two kittens is the visuomotor coupling. In subsequent tests, passive kittens didn't show a visually guided paw placement response when held approaching a table surface, and failed to discriminate shallow and deep in the visual cliff test, while active kittens appeared normal (Hein et al., 1970; Held and Hein, 1963).

Interestingly, different visually guided behaviors, or different components of the same behavior, are developed independently, which require the experience of that specific corresponding visuomotor coupling, as later shown by Held and Hein. Kittens reared in normal environment but don't have sight of their own limbs successfully developed paw placement response, however, the accuracy of the placement is greatly impaired (Hein and Held, 1967). Similar results were later observed in monkeys as well (Bauer and Held, 1975). Moreover, the development of this paw placement behavior is also eye dependent, as if only one eye was exposed with proper visuomotor coupling, the kitten only show the behavior with that eye open, but not with the other eye (Hein et al., 1970). Thus, "the system for visual guidance of movement consists of components which can be acquired independently".

Motor-related signals in V1

As illustrated by Rao and Ballard, visual predictions could be made based on spatial/temporal adjacent visual inputs. Along the same line of thinking, visual predictions could also be made based on motor-related signals, that is, the animal's own motor commands. It has been proposed that the brain sends an "efference copy" (also called "corollary discharge") of the motor commands and use it for sensorimotor integration.

In recent years, there has been an accumulating body of works indicating that neural activity in V1 is strongly modulated (Fu et al., 2014; Niell and Stryker, 2010) and driven (Keller et al., 2012; Saleem et al., 2013) by self-generated movement. These motor-related signals are not only much more prominent than visual stimulus-evoked responses alone, but also exist even without visual stimulus (Keller et al., 2012). While this led people to rethink the classical definition of sensory cortices, it seems that the long proposed sensorimotor integration could already happen at a rather low-level cortical area such as V1.

Moreover, there are a subset of cells in V1 selectively respond to the mismatch between predicted and actual visual input (Keller et al., 2012). By introducing brief halts to perturb the normal visual

flow feedback when mice running in a virtual reality environment, cells in V1 respond strongly to this brief halt. This mismatch response cannot be explained by visual stimulus alone as it clearly depends on the integration of both visual stimulus and motor-related signals. If this mismatch response is indeed based on the learned correlation between forward running and coupled backward moving visual flow, then it is very likely that this mismatch response depend on the prior visuomotor experience of the animal.

In the present study, we adapted the aforementioned “kitten carousel” training paradigm to mice with virtual reality environment, that is, with either coupled or non-coupled visuomotor experience, and then image the neural activity in V1, to see whether visuomotor coupling experience affect the mismatch response in mice V1, and try to identify a local microcircuit that underlie the computation of the mismatch response.

Results[1]

Mice were dark-reared from birth and only exposed to visual stimulation in six two-hour training sessions every other day over the course of 12 days, starting on postnatal day 32 (**Figure 1A**). During the training sessions each mouse was trained either in a coupled visuomotor condition (coupled trained: CT), in which the visual flow feedback was coupled to the mouse's own locomotion, or in a non-coupled condition (non-coupled trained: NT) in which visual flow was independent of the mouse's locomotion (**Figure 1B**). Mice were head-fixed on a spherical treadmill (Dombeck et al., 2007) surrounded by a toroidal screen that provided visual flow feedback in the form of full-field vertical gratings on the walls of a virtual corridor. To match the visual experience of both groups, mice were trained in pairs (one CT and one NT mouse) in two separate virtual reality environments such that the locomotion of the CT mouse was used to control the visual flow of both virtual environments (**Figure 1B**). In this way, both CT and NT mice experienced identical visual flow. A third group of mice was reared and trained in complete darkness (dark trained, DT). After the 6 training sessions, we recorded neural activity in V1 of all 3 groups of mice by two-photon imaging of a genetically encoded calcium indicator GCaMP5 (Akerboom et al., 2012) or GCaMP6f (Chen et al., 2013) during different visual flow feedback conditions in 5 imaging sessions every other day, starting on postnatal day 44. After the second imaging session is finished, mice were transferred to a normal dark-light cycle environment (**Figure 1A**). Imaging sessions for all groups of mice consisted of 1 or 2 repetitions of approximately 8 minutes (500 s) of locomotion coupled to visual flow feedback (closed-loop session), and 2-3 replays of the same visual flow patterns during an open-loop session to quantify visual responses. To probe for feedback mismatch responses, we briefly halted visual flow for 1 second at random times during the closed-loop session (referred to as mismatch), while in open-loop sessions these halts of visual flow were also replayed to the mice, which we refer to as playback halts. Note that analysis of playback halts was restricted to times when the mouse was not running (see Materials and methods). Mice were free to run during the entire experiment, including open-loop sessions and did so spontaneously. In early sessions, mice that exhibited low locomotor activity were prompted to run using air-puffs to the neck. CT and NT mice exhibited similar locomotion behavior during both training and imaging sessions (**Figures S1A and S1B**).

We expressed GCaMP5 in C57BL/6J mice and GCaMP6f in vGAT-Cre (Vong et al., 2011) x Ai14 (Madisen et al., 2010) mice using an AAV2/1-EF1α-GCaMP vector (see Methods). We chose to use vGAT-Cre x Ai14 mice which inhibitory neurons express tdTomato to identify excitatory and

[1] Part of the Results section also appear in the manuscript of the paper which has been submitted to Cell, with modifications.

inhibitory neurons in our imaging data. We found that the overlap between green and red labelled cells are very small, resulting 96.8% ± 0.7% (mean ± s.e.m.) of GCaMP6f labelled neurons were excitatory (**Figures S1C and S1D**). Thus, we pooled all the data from wild-type C57BL/6J mice and vGAT-Cre x Ai14 mice and referred them as excitatory neurons. In total, we recorded from 2259 excitatory neurons in CT mice (996 putative excitatory and 1263 identified excitatory neurons) and 2104 excitatory neurons in NT mice (764 putative excitatory and 1340 identified excitatory neurons).

Responses in excitatory neurons

We found that in CT mice, a considerable fraction of excitatory neurons responded to mismatch (865 of 2259 neurons or 38.3%; **Figures 1C and 1D**) resulting in a large population mismatch response (**Figure 1E**). In CT mice, mismatch responses cannot be explained by visual input alone as there was no population response to playback halt (**Figure 1C and 1E**; note, mismatch and playback halt are identical visual stimuli). This is consistent with what we previously found in normally reared mice (Keller et al., 2012). In NT mice, the fraction of neurons that responded to mismatch was smaller (425 of 2104 neurons or 20.2%) and the population response to mismatch was weaker than in CT mice (**Figure 1E and S1E**). Interestingly, in NT mice the response to mismatch was of similar magnitude as the response to playback halt (**Figure 1E**) and individual neurons often responded to both mismatch and playback halt (**Figures S1F and S1G**). With increasing mismatch response, neurons in CT, but not NT, mice became increasingly selective for mismatch (**Figure S1H**). Thus, whereas in CT mice, mismatch responses cannot be explained by visual input alone and require integration of motor-related and visual inputs, mismatch responses in NT mice are predominantly visually driven. In both CT and NT mice, the response reliability of mismatch responsive neurons increased with average amplitude of the mismatch response. On average mismatch neurons responded to 37.5% of mismatches in CT mice and 33.8% in NT mice (**Figure S1I**). A subset of neurons, separate from mismatch neurons, responded with a decrease in activity to mismatch as well as playback halts (**Figure 1D and S1J**). This response type is consistent with a visual response driven by visual flow: upon cessation of the visual flow, the neuron decreases its response.

However, the running-onset response during the closed-loop session (referred to as running-onset response) and the visual flow onset responses during open-loop sessions (referred to as playback-onset response) were similar between CT and NT mice (**Figure 1F**). Thus, the differences in mismatch responses between CT and NT mice cannot be explained by differences in average visual or motor-related input to V1. In dark trained mice, running-onset responses were normal, but mismatch and playback halt responses were smaller (**Figure S2**). This suggests that visual and motor-related inputs are maintained independently, and that visuomotor coupling is necessary for the development of normal integration of visual and motor-related inputs.

The next thing we tried to find out is how is the mismatch response generated? To do it the mismatch cell needs to receive both motor-related input and visual input, and the simplest model for this would be that these two inputs have opposite signs, one being excitatory and the other one being inhibitory. Motor-related inputs have been shown to drive activity in mouse V1 (Keller et al., 2012; Saleem et al., 2013), thus mismatch cells should receive inhibitory visual input, and this feed-forward visual inhibition would need to be relayed by local inhibitory neurons (**Figure 2A**). In this model, inhibitory and excitatory inputs are balanced when predictions match feed-forward input. At mismatch onset, a decrease in visual feed-forward inhibition would then allow the excitatory motor-related input to activate the neuron. To test this, we computed the correlation of the activity of each neuron with visual flow and with running speed during the open-loop sessions. As running and visual flow are independent in open-loop sessions, the activity of a neuron that receives net inhibitory visual input and net excitatory motor-related input would have a negative correlation with visual flow and a positive correlation with running speed and vice versa. Plotting the distribution of the correlations of all neurons revealed that neurons with a strong mismatch response, had a negative correlation with visual flow and a positive correlation with running speed, on average (**Figure 2B**). When comparing the entire population of neurons, we found that in CT mice, neurons with a positive correlation with running speed tended to have a negative correlation with visual flow, whereas in NT mice neurons with a positive correlation with running speed tended to also have a positive correlation with visual flow. We quantified this interaction for every mouse as the angle (A) of the first principal component of the correlation scatter plot and found that, in CT mice, this angle was on average negative (-41° ± 10°, mean ± s.e.m.), whereas in NT mice it was on average positive (9° ± 13°, mean ± s.e.m.; **Figures 2B and 2C**). This suggests that visuomotor coupling establishes a balance between inhibition and excitation, such that those layer 2/3 excitatory neurons that are strongly activated by running are also strongly inhibited by visual input.

Responses in inhibitory neurons

As most long-range input to V1 are excitatory, to make the aforementioned circuit work, visual input needs to be relayed by a local inhibitory interneuron in V1, such that visual input excite this interneuron, and it further inhibit the mismatch cell. To test this, we repeated the same training and imaging paradigm using 4 different Cre mouse lines to selectively express GCaMP6f (AAV2/1-EF1α-DIO-GCaMP6f-WPRE) in somatostatin (SST) (Taniguchi et al., 2011), vasoactive intestinal polypeptide (VIP) (Taniguchi et al., 2011), parvalbumin (PV) (Hippenmeyer et al., 2005), or neuropeptide-Y (NPY) (Gong et al., 2007) interneurons. These SST-Cre, VIP-Cre and PV-Cre lines target approximately 80% of interneurons in mouse V1 and are largely non-overlapping (Pfeffer et al., 2013).

We found that among all the interneuron subtypes we tested as well as excitatory neurons, SST interneurons showed highest correlation with visual flow (**Figure 3**). Moreover, only SST interneurons responded, on average, with a drop in activity to both mismatch and playback halt (**Figure 4A**). This drop in activity on visual flow halt was independent of visuomotor experience as it was present in both CT (5 mice, 118 neurons) and NT mice (5 mice, 157 neurons), indicating that the visual input onto SST neurons is established independently of motor-related input. Note that although running onsets in closed-loop session strongly activate SST interneurons (**Figure 4B**), but running-onset responses were almost absent in darkness (**Figure S3A**), indicating the strong activation seen in closed-loop session is largely due to visual input.

The responses of VIP interneurons were also independent of visuomotor experience. In both CT and NT mice, they responded with an increase of activity to mismatch but not to playback halt (**Figure 4C**; CT: 3 mice, 189 neurons; NT: 3 mice, 137 neurons). Since SST and VIP interneurons mostly project reciprocally in the cortex (Pfeffer et al., 2013), mismatch responses may result from the combination of a running-related excitatory input to VIP interneurons (Fu et al., 2014) and a relief from SST interneuron mediated inhibition. Interestingly, running-related input to VIP interneurons was strongly experience dependent. VIP interneurons were only driven by running onset during closed-loop sessions in CT but not in NT mice (**Figure 4D**). Consistent with the strong reduction of running-onset responses in SST interneurons in darkness, a running-related input to VIP interneurons in NT mice was unmasked in darkness (**Figure S3B**). Taken together, our findings suggest that the inhibitory connection from SST interneurons onto VIP interneurons is stronger in absence of visuomotor experience.

Responses in both PV interneurons (CT: 5 mice, 498 neurons; NT: 6 mice, 344 neurons) and NPY interneurons (CT: 3 mice, 189 neurons; NT: 3 mice, 137 neurons) were behavioral state and visuomotor-experience dependent. These two interneuron subtypes were activated by mismatch in CT mice, but unresponsive to mismatch in NT mice and unresponsive to playback halt in both CT and NT mice (**Figures 4E, S3C-E**). This highly selective response to mismatch in CT mice could be a direct consequence of the stronger activation of the excitatory neuron population in CT mice in response to mismatch (**Figure 1E**). Either excitatory neurons recruit PV and NPY interneurons only above a given activity level or the calcium dynamics in PV and NPY interneurons are such that we are unable to measure activity changes below a given threshold. Note however, that such a simple measurement threshold cannot account for the observation that in CT mice the population response of excitatory neurons to running onset is smaller than that to mismatch (**Figures 1E, 1F**), but the running-onset response of PV interneurons is larger than that to mismatch (**Figures 4E, 4F**). One potential consequence of a selective activation of PV interneurons in CT mice is that the PV

activation could lead to a response normalization in excitatory neurons (Wilson et al., 2012) that narrows the population response to mismatch. Consistent with this, we found that the distribution of mismatch responses is narrower in CT mice (**Figure S3F**). This narrowing of the distribution of mismatch responses could function to make mismatch responses more selective to one particular type of mismatch.

Our data indicate that layer 2/3 excitatory mismatch neurons and VIP interneurons receive excitatory, motor-related input, while SST interneurons receive strong excitatory visual input. Consistent with the finding that SST interneurons receive strong input from surrounding excitatory neurons (Adesnik et al., 2012; Fino and Yuste, 2011; Jiang et al., 2015), we found that excitatory neurons whose activity correlates positively with visual flow (CT: 24% or 539 of 2259 of neurons; NT: 24% or 513 of 2104 neurons) exhibit a decrease in activity on mismatch similar to SST interneurons (**Figure S4**). Based on the connectivity motif of excitatory neurons, SST and VIP interneurons (Pfeffer et al., 2013; Pi et al., 2013), we propose a schematic model circuit to explain mismatch responses in layer 2/3 excitatory neurons (**Figure 5A**). SST interneurons target the apical dendrites of layer 2/3 excitatory neurons (Markram et al., 2004). A reduction of feed-forward visual input onto SST interneurons during mismatch thus relieves the apical dendrite of inhibition, and would allow excitatory motor-related input to activate the neuron. Based on this model we predict that both SST interneuron activation and inhibition should lead to a decrease of the mismatch response in excitatory neurons, but should have opposing effects on running-related activity in excitatory neurons (**Figure 5B**). To test this, we manipulated the activity of SST interneurons using DREADDs (Armbruster et al., 2007). We injected either AAV-EF1α-DIO-hM4D(Gi)-mCherry or AAV-EF1α-DIO-hM3D(Gq)-mCherry into V1 of normally reared SST-Cre mice. In addition, we unconditionally transfected neurons with GCaMP6f to record mismatch and running related activity in putative excitatory neurons. Note that in these experiments we cannot exclude the possibility that some of these putative excitatory neurons are non-SST interneurons. We found that DREADD inhibition of SST interneurons led to an increase in running-related activity in excitatory neurons, while DREADD activation of SST interneurons led to a decrease in running-related activity (**Figure 5C**). In addition, both inhibition and activation of SST interneurons led to a decrease in the mismatch response of excitatory neurons (**Figures 5D and 5E**). These results are consistent with a model of mismatch computation in which mismatch responses in layer 2/3 neurons are the result of a relief of SST interneuron mediated inhibition. To test the effect of a transient manipulation of SST and VIP activity on mismatch responses we injected AAV-EF1α-GCaMP6f and either AAV-EF1α-DIO-ChrimsonR-tdTomato (Klapoetke et al., 2014) or AAV-CAG-FLEX-ArchT-tdTomato (Han et al., 2011) into V1 of normally reared SST-Cre mice and VIP-Cre mice. We then identified putative excitatory mismatch

neurons based on their responses to mismatch events in closed-loop sessions (in the following simply referred to as mismatch neurons) and measured the responses of these neurons to brief (1 s) activation or inhibition of SST or VIP interneurons (see Methods). We found that activation of SST interneurons resulted in an inhibition of mismatch neurons that was strong enough to fully suppress mismatch responses in mismatch neurons when SST interneurons were activated concurrently with a mismatch event (**Figure 6A**). Consistent with this, inhibition of SST neurons resulted in an activation of mismatch neurons and concurrent inhibition of SST interneurons with a mismatch event resulted in increased mismatch responses (**Figure 6B**). Conversely, activation of VIP interneurons resulted in an activation of mismatch neurons and an increase of the mismatch response when VIP interneurons were activated concurrently with a mismatch event (**Figure 6C**). Finally, inhibition of VIP interneurons resulted in an inhibition of mismatch neurons that was strong enough to suppress mismatch responses (**Figure 6D**). All of these effects are stronger for mismatch neurons than for putative excitatory neurons that do not respond to mismatch (**Figure S4**). In summary, these results are consistent with the classical cortical SST-VIP disinhibitory circuit (Pfeffer et al., 2013; Pi et al., 2013), and suggest that this circuit plays a central role in mismatch computation with mismatch neurons under inhibitory control of SST interneurons. Thus, the relief of SST-mediated feed-forward visual inhibition combined with a top-down motor-related excitatory drive can account for visuomotor mismatch responses in layer 2/3 excitatory neurons.

Response change in the time course

Given that both CT and NT mice learned to perform visuomotor tasks over the course of a few days, visuomotor coupling should rapidly restore normal visuomotor processing in V1. To quantify the change in neural processing in V1 with the exposure to visuomotor coupling, we measured mismatch responses in both CT and NT mice over the course of 8 days following restoration of visuomotor coupling (exposure to both open-loop and closed-loop conditions and normal visuomotor experience with the transfer to rearing in a normal light/dark cycle; **Figure 1A**). We found that mismatch responses of excitatory neurons in CT and NT mice equalized rapidly with normal visuomotor experience (**Figures 7A** - **7C**). The population mismatch responses of SST and VIP interneurons remained stable throughout the course of the experiment for both CT and NT mice (**Figures 7D and 7E**). This is consistent with the idea that the mismatch response of VIP and SST interneurons developed independent of visuomotor coupling. Similar to excitatory neurons, mismatch responses in PV and NPY interneurons equalized after restoration of normal visuomotor coupling (**Figures 7F** and **S6A**). Interestingly, we found not only an increase of mismatch responses in NT mice with exposure to closed-loop sessions and normal visuomotor experience, but also a decrease of mismatch responses in CT mice with exposure to open-loop sessions and normal visuomotor

experience. Similarly, we found that for the distribution of visual flow and running speed correlations, the angle of the first principle component (**Figures 2B and 2C**) equalized and approached zero for both CT and NT mice (**Figures 7G and S6B**). Altogether, these results suggest that the artificial restriction of visuomotor coupling to only a subset of movements (forward locomotion and eye movements) leads to an overrepresentation of the visuomotor processing of these movements that needs to be unlearned for the restoration of normal visuomotor behavior. This is consistent with the finding that a lack of visuomotor coupling for a specific range of movements leads to behavioral impairments that are specific to those movements (Hein and Held, 1967).

Behavior

We performed a similar visual cliff test for the first batch of wild-type CT and NT mice as in Held and Hein's study (Held and Hein, 1963). Mice were tested both after finishing the second imaging session (last session before transferring to normal rearing environment) and the fifth imaging session. In contrast to the results of Held and Hein's, we found both CT and NT mice failed at the visual cliff test, in both before and after normal visuomotor exposure, while normal-reared mice always chose the safe side (**Table S1**). In addition, we found both CT and NT mice were reluctant to step down from the ridge, resulting many time outs and limited total number of trials (**Table S1**), as oppose to the presumption of the visual cliff test that mice will try to avoid elevated places in general. This potential confound made it hard to interpret the results, however, it seems that both CT and NT mice have impaired visual functions and 6 days of exposure to normal environment is not enough to fully recover the normal behavior in visual cliff test.

We also tested if CT and NT mice can learn to perform visuomotor tasks after exposure to normal visuomotor coupling. After the coupled and non-coupled training, mice were trained either to navigate a 2-dimensional (2D) virtual environment or to detect mismatch (see Methods). Both CT and NT mice learned to perform the 2D virtual locomotion task over the course of 6 training sessions of 1 hour each (**Figures S5A, S5B**). Also, both CT and NT mice learned to report the occurrence of mismatch over the course of 3-5 training sessions of 1 hour each (**Figure S5C**). These results suggest that NT mice could quickly adapt and establish normal visuomotor processing with exposure to proper visuomotor coupling.

To quantify the behavioral response to mismatch, we also measured pupil dilation at the onset of mismatch. Mice showed a measurable pupil dilation response with a delay of approximately 450 ms after the neural response to a mismatch (400 ms for CT, 500 ms for NT; see Methods; **Figure 7H**). This pupil dilation response was larger in CT mice than in NT mice, and may reflect a startle

response. Similar to the time course effect in neural activity, the pupil dilation response also equalized after exposure to normal visuomotor experience (**Figure 7I**).

Gene expression

To explore the potential difference in gene expression in the visual cortex of CT and NT mice, we planned to adopt a genetically defined cell-type specific gene profiling approach, called translating ribosome affinity purification (TRAP) method (Heiman et al., 2008). As a trial experiment, we first tried gene profiling on total RNA extracted from V1 tissue after coupled or non-coupled visuomotor training. No genes were found to have significant difference in expression fold-change ($p < 0.01$, fold-change > 2) after three two-hour training sessions between CT and NT mice (**Figure S7**). However, when compared between male and female mice, we could show that there are five genes stands out the criteria (**Figure S7**), all of them locate on the X or Y chromosomes (**Table S2**). The results suggest that our gene profiling microarray system does seem to work, but total RNA preparation might be too crude to identify differences in gene expression between CT and NT treatments.

Discussion

In the present study, we have shown that the development of mismatch responses in mouse V1 depends on the prior visuomotor experience, and such response could be resulted from the transient release from the inhibition of local SST interneurons. We suggest that a subset layer 2/3 computes the difference between predicted and received visual flow, based on excitatory motor-related input and inhibitory visual input, and the balance between the two is tuned by visuomotor experience. Our results provide another piece of evidence in favor of the predictive coding framework of sensory cortex function, as opposed, or a supplement, to the prevailing representation framework.

One common misunderstanding of the term “mismatch” we use here is that it is something “bad” and needs to be corrected. This is not necessarily true. In the context of predictive coding framework (Rao and Ballard, 1999), sensing the mismatch helps the brain to focus on the meaningful fraction of sensory stimuli while ignoring the rest. Thus, the mismatch is something the brain needs “pay attention” to, but not always needs to correct. Of course, as the internal model is still plastic after established, and it could adapt to some mismatch if it happens every time thus not interesting anymore. Note that as predictive coding framework is also based on a multiple hierarchical structure, internal models could be updated only at lower levels and in short terms (e.g. sensory adaptation).

Another common misunderstanding of the mismatch paradigm we use in this study and the previous study (Keller et al., 2012) is that this kind of “mismatch” is not likely to happen in real life, thus why would the visual cortex evolutionarily develop a computational circuit dedicated to detect such situation? First, in terms of visuomotor mismatch, there will be two kinds of it by definition: either received visual input is less (slower), or more (faster) than expected. In extreme cases, it would be either the animal is not moving but see moving gratings, or that the animal is running but visual flow stops. The former would be the same as a classical visual stimulus and has been described in early visual neuroscience research (Hubel and Wiesel, 1959). To demonstrate the difference between predictive coding and representation framework, we chose the latter kind of mismatch as responses to these mismatch cannot be explained by the representation framework. Second, the sudden halt of full-field visual flow is just a simplified paradigm we chose, potentially maximize the response we record. Local mismatch could happen in real life (e.g. a small object moving at the same speed as you move), and as shown in a recently published paper from our lab, mismatch cells also have receptive fields, which their sizes match to those classified as pure “visual responsive” cells and are also organized in the same retinotopic structure (Zmarz and Keller, 2016).

There are studies in recent years reported that motor-related excitatory input to V1 serve as a kind of neuromodulation, which amplify visual responses without changing the basic response properties (Fu et al., 2014; Niell and Stryker, 2010). We don't think the motor-related signals are just modulatory. First, the running-related gain associated with visual responses (approximately a factor of 2 to 3) cannot account for the difference between the playback halt response and the mismatch response (roughly a factor of 9)(Zmarz and Keller, 2016). Hence to describe mismatch responses as a visual response with a running-induced gain would require invoking a stimulus specific change in running-related gain (a different running-related gain for classical visual stimuli and the playback halt stimulus, respectively). Second, the amplitude of mismatch responses scales linearly with the difference between running speed and visual flow speed (Keller et al., 2012; Zmarz and Keller, 2016). Moreover, this relationship of mismatch response with the difference between running speed and visual flow is identical when computed on playback data (where running speed and visual flow vary independently and continuously) or mismatch events (where the is an abrupt halt of visual flow). This means the stimulus driving the mismatch signal is the difference of visual flow and running speed, not the abrupt halt of visual flow. This is also exemplified by the fact that we can use playback data to estimate the parameters of the integrate-and-fire neuron model (**Figure 2E,F**) and predict the responses to mismatch events. Hence, also a nonlinear combination of a running-related signal and a visual response to the playback-halt stimulus cannot explain mismatch responses, as such a combination of two excitatory signals could not easily result in a linear increase with the difference between visual flow speed and running speed.

Our results suggest that functional mismatch neurons receive both excitatory motor-related input and inhibitory visual input, the latter of which is mediate by SST interneurons. As we show that in NT mice this mismatch signals are impaired, precise targeting the two input onto the same cell might require the normal exposure of such visuomotor experience. On the contrary, mismatch responses in SST and VIP interneurons do not depend on visuomotor experience (**Figure 4A,C**), suggesting that visuomotor experience mainly modifies the synaptic inputs onto the excitatory neuron. The balance between excitation and inhibition is established in this way and further maintained and updated by visuomotor experience (**Figure 7C-F**).

What are the potential brain areas that send motor-related and visual input to the V1 model circuit we proposed there? Feed-forward visual input onto SST interneurons likely comes from surrounding, visually-driven layer 2/3 excitatory neurons (Adesnik et al., 2012; Fino and Yuste, 2011; Jiang et al., 2015). The source of the motor-related excitatory input is less clear. V1 receives input from various other cortical areas, including direct projections from motor-related areas like the anterior cingulate cortex (Miller and Vogt, 1984; Vogt and Miller, 1983; Zhang et al., 2014) and the retrosplenial cortex

(Miller and Vogt, 1984; Vogt and Miller, 1983). These projections could convey the signal of predicted visual flow based on the motor output of the animal.

The idea of sensorimotor integration, efference copy and internal model has long been suggested, and many theoretical works argue that making predictions and error correction is one of the essential function of the brain. Along the same line of thinking, we propose that the comparison of feed-forward input with a top-down prediction may be a general principle of cortical function, where predictions from higher areas are continuously compared to signals from lower areas, and mismatches between the two are used to refine these predictions (Clark, 2013; Friston, 2010). It is intriguing to speculate that impairments in this comparison may underlie cortical dysfunctions where the balance between predictions and feed-forward input is systematically perturbed (Frith et al., 2000; Sinha et al., 2014), as it could account for many symptoms observed in autism spectrum disorders and schizophrenia. Thus, the circuit mechanism for computing visuomotor mismatch we described here could potentially be a testable model for studying pathology and treatments for those diseases.

Figures and tables

Figure 1

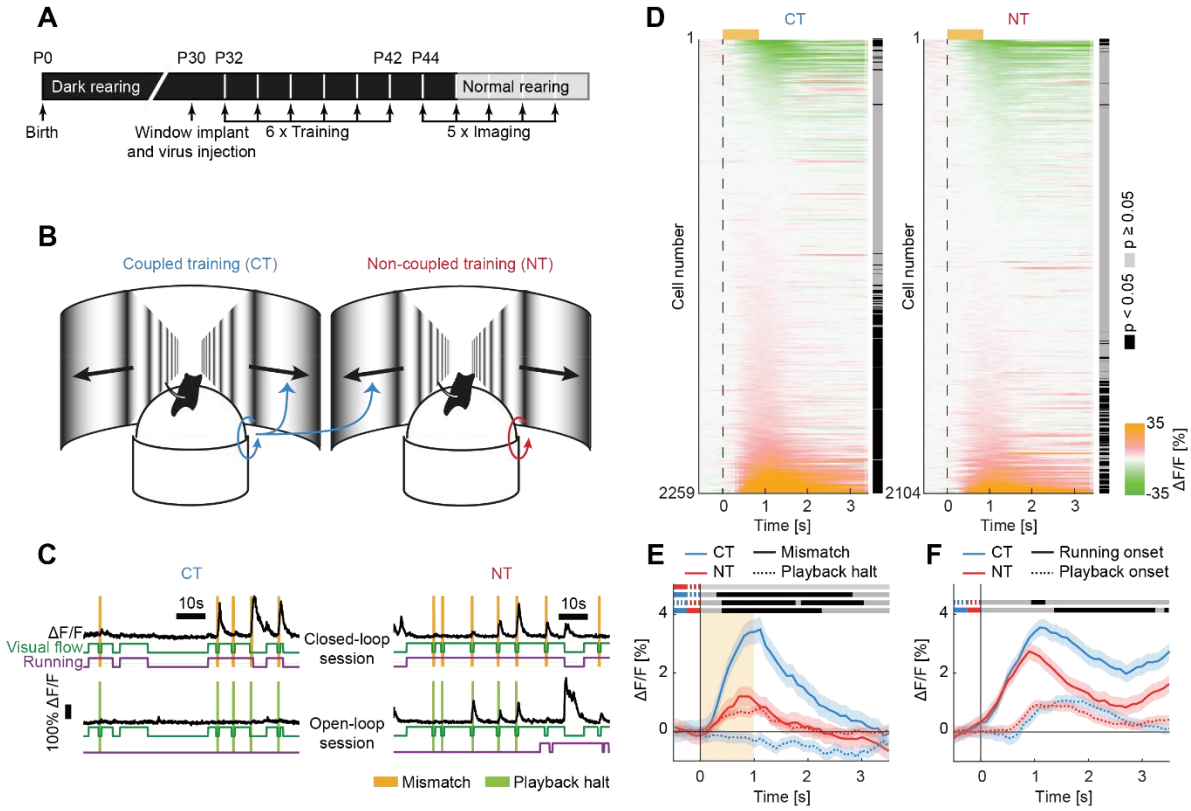

Figure 1. Mismatch responses in excitatory neurons depend on visuomotor experience.

(A) Experimental timeline. Mice were dark-reared from birth. AAV injection and imaging window implantation occurred on postnatal day 30 (P30). From P32 to P42, mice had 6 training sessions in either coupled (coupled trained: CT), non-coupled (non-coupled trained: NT), or dark (dark trained: DT) conditions, followed by 2 to 5 imaging sessions beginning at P44 and spaced by 2 days. Some of the mice were put on a normal 12 h/12 h light/dark cycle after the second imaging session.

(B) Schematic of the training setup. Mice were trained in pairs; visual flow (black arrows) on both training setups was coupled to the locomotion of the CT mouse (blue arrows). The NT mouse was free to run but had no influence on the visual flow it was seeing.

(C) Sample fluorescence traces (ΔF/F, black lines) of an excitatory neuron in a CT (left) and a NT (right) mouse, during a closed-loop (top traces) and an open-loop session (open-loop sessions consisted of a replay of the visual flow generated during the preceding closed-loop session, bottom traces). Vertical bars indicate mismatch (orange) and playback halt (green) events. Binarized visual flow (green) and running speed (purple) are indicated below the fluorescence traces. In CT mice, we found neurons that selectively respond to mismatch, whereas in NT mice, neurons that responded

to mismatch also responded to corresponding playback halts in open-loop sessions. Note that all data presented in this and the following panels are from the first imaging day.

(D) Average mismatch response (ΔF/F) of all neurons in CT mice (left, 9 mice, 2259 neurons) and NT mice (right, 9 mice, 2104 neurons), sorted by amplitude of mismatch response. Black and grey shading to the right indicates significance of responses (grey: $p \geq 0.05$, black: $p < 0.05$, Mann-Whitney-U test; see Methods). Orange bar marks the duration of mismatch. In CT mice, the fraction of neurons with a significant mismatch response was larger than in NT mice (CT: 40% ± 5%; NT: 26% ± 5%, $p = 0.03$, Mann-Whitney-U test; see Methods).

(E) The average population response (ΔF/F) to mismatch (solid) was stronger in CT (blue) than in NT (red) mice. Population response to playback halt was negligible in CT mice, but was as large as the mismatch response in NT mice (dashed lines). Orange area indicates duration of mismatch; shading indicates s.e.m. The data in the different curves are compared bin-by-bin (100 ms bins) using a Student's t test. Bins with a significant difference ($p < 0.01$) are marked by a black line above the curves; those without are marked as light gray (see Methods). Each comparison is marked by a pair of line segments to the left, corresponding in color and line style to the data plotted, indicating which two curves are being compared.

(F) Same as in (**E**), but for running onset in closed-loop sessions (solid lines) and playback onset in open-loop sessions (dashed lines, see Methods). Shading indicates s.e.m.

Figure 2

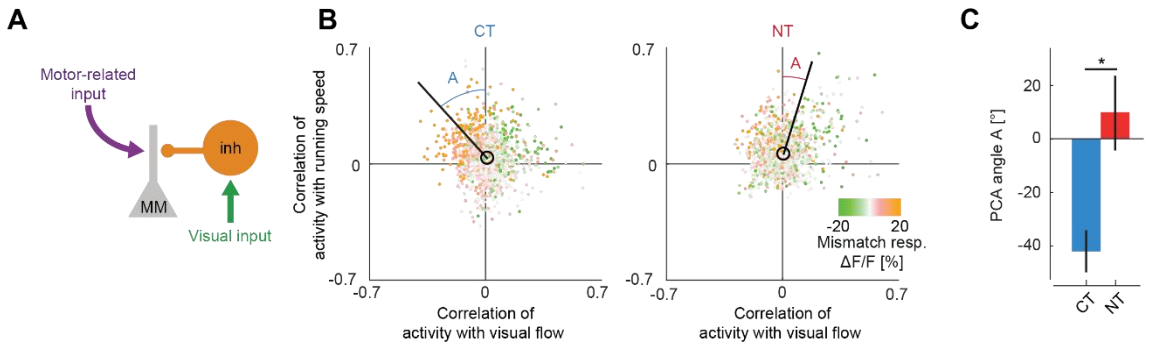

Figure 2. Mismatch responses can be explained as a difference between an excitatory motor-related input and an inhibitory visual input.

(A) Circuit model in which an excitatory mismatch neuron (MM, grey) integrates excitatory motor-related input and inhibitory visual input relayed by a local inhibitory interneuron (orange) to compute the difference between predicted and actual visual flow.

(B) Correlation coefficients between neural activity (ΔF/F) of layer 2/3 excitatory neurons with running speed and with visual flow in CT (left; 9 mice) and NT (right; 9 mice) mice during open-loop sessions. Each dot represents a single neuron (CT: 2259 neurons; NT: 2104 neurons). Dot color indicates the amplitude of the mismatch response. Black circles indicate the mean correlation values. The angle A indicated by the solid black line is the average angle between the first principle component of the distribution and the y-axis (see Methods). Note that all data presented in this and the following panels are from the first imaging day.

(C) Mean angle of the first principle component relative to the y-axis of the distribution of correlation coefficients as in (**B**) for CT (n = 9) and NT mice (n =9). Error bars indicate s.e.m., Mann-Whitney-U test, p = 0.04.

Figure 3

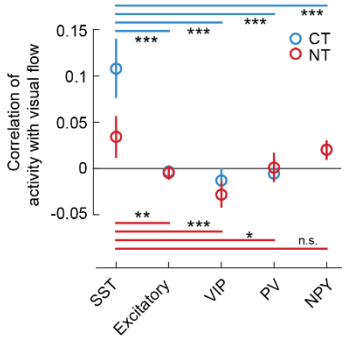

Figure 3. SST interneurons are strongly driven by visual flow.

Average correlation of neural activity with visual flow during open-loop sessions for excitatory neurons (average correlations: CT: 0.00, NT: -0.01) and SST (CT: 0.13, NT: 0.04), VIP (CT: -0.01, NT: -0.03), PV (CT: -0.01, NT: 0.00) and NPY (CT: 0.02, NT: 0.02) interneurons in CT and NT mice. Average correlation of activity with visual flow was highest for SST interneurons. Error bars indicates s.e.m. *: $p < 0.05$, **: $p < 0.01$, ***: $p < 0.001$, n.s., not significant, $p \geq 0.05$, Student's t test.

Figure 4

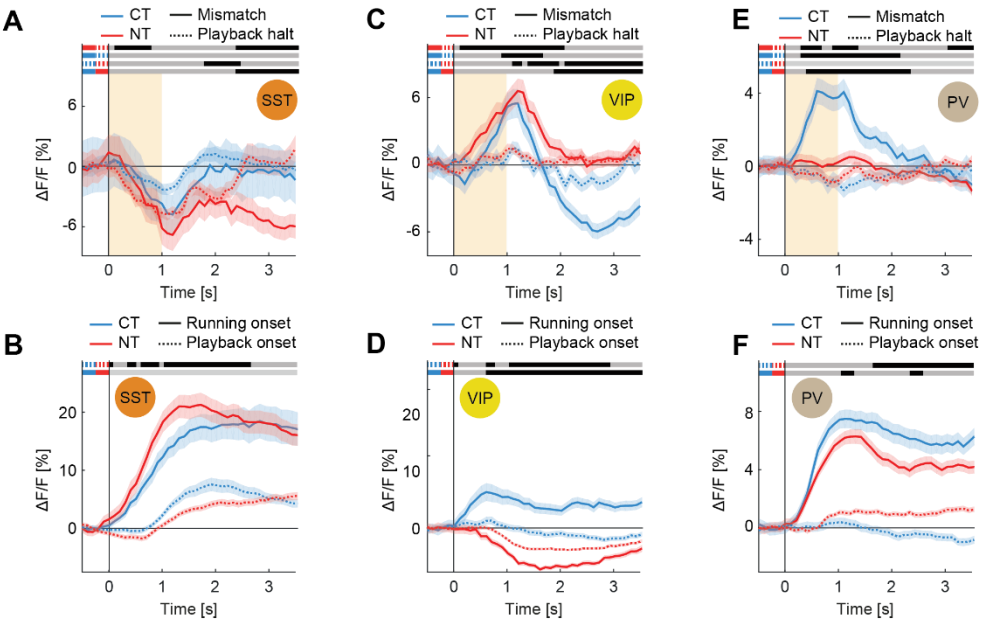

Figure 4. Experience dependent visuomotor integration in inhibitory interneurons.

(A) Average population responses to mismatch (solid line) and playback halt (dashed line) for SST interneurons from CT (blue, 5 mice, 118 neurons) and NT (red, 5 mice, 157 neurons) mice. For both CT and NT mice, SST interneurons responded with a decrease in activity to mismatch and playback halt. Orange area indicates duration of mismatch; shading indicates s.e.m. Note that all data presented in panels **A**-**F** are from the first imaging day. The data in the different curves are compared bin-by-bin (100 ms bins) using a Student's t test. Bins with a significant difference ($p < 0.01$) are marked by a black line above the curves; those without are marked as light gray (see Methods). Each of the four comparisons is marked by a pair of line segments to the right, corresponding in color and line style to the data plotted, indicating which two curves are being compared.

(B) Same as in (**A**), but for running onset in closed-loop sessions (solid lines) and playback onset in open-loop sessions (dashed lines).

(C and D), Same as in (**A and B**), but for VIP interneurons (CT: 3 mice, 189 neurons; NT: 3 mice, 137 neurons). VIP interneurons responded with an increase in activity independent of experience but did not respond to playback halt.

(E and F) Same as in (**A and B**) but for PV interneurons (CT: 5 mice, 498 neurons; NT: 6 mice, 344 neurons). The mismatch response in PV interneurons was strongly experience dependent.

Figure 5

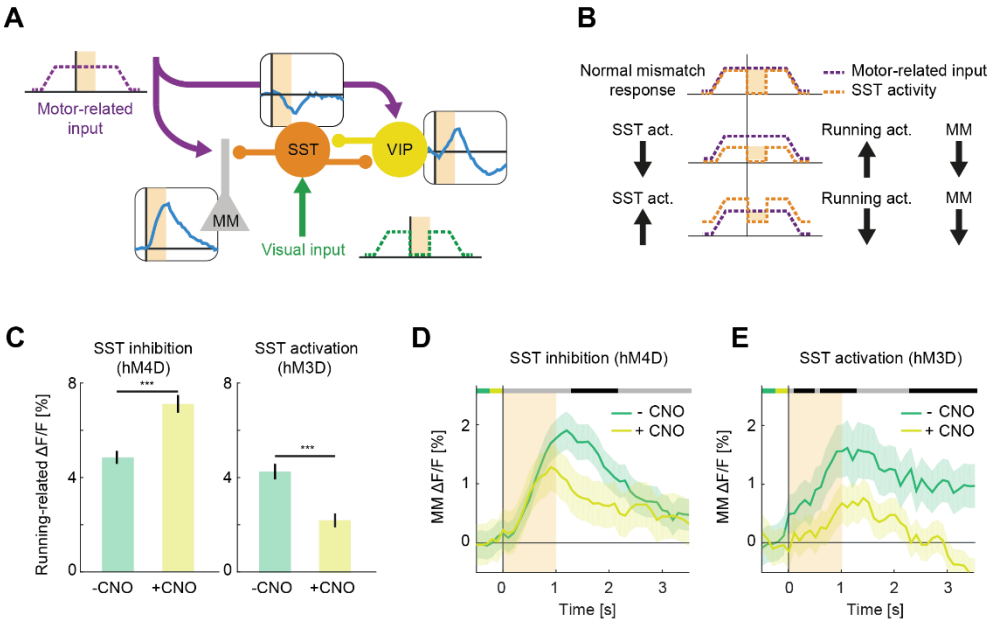

Figure 5. A drop in SST activity leads to a mismatch response in excitatory neurons.

(A) Schematic of a model circuit describing the computation of mismatch responses in layer 2/3 of V1. Excitatory neurons and VIP interneurons receive excitatory motor-related input (purple arrow; dashed purple line depicts idealized running profile around a mismatch, indicated by orange shading). SST interneurons receive feed-forward visual flow input (green arrow; dashed green line depicts idealized visual flow around a mismatch, indicated by orange shading). Blue lines next to neurons depict average mismatch responses of excitatory neurons (**Figure 1E**), SST (**Figure 4A**) and VIP (**Figure 4B**) interneurons from CT mice. During mismatch, visual flow is halted and the activity of SST interneurons decreases, thereby disinhibiting the apical dendrites of mismatch neurons and allowing the excitatory motor-related input to activate the neuron. VIP interneurons amplify this effect by further suppressing SST interneuron activity.

(B) Predicted effects of pharmacogenetic manipulation of SST interneurons on excitatory neurons. Idealized activity profiles of excitatory motor-related activity (purple line) and SST interneuron activity for a short period of running during a closed-loop session including a mismatch (onset marked by vertical line). In normal conditions (top), SST interneuron activity balances the motor-related input and the mismatch response of excitatory neurons is maximal (mismatch-triggered difference between excitatory and inhibitory input, orange shading). Inhibition of SST interneurons (middle) should result in a smaller mismatch-induced difference in inhibition and therefore a smaller mismatch response as well as increased running-related activity. Excitation of SST interneurons

(bottom) should also result in smaller mismatch responses due to an over-inhibition of excitatory neurons, but decreased running-related activity.

(C) Mean running related activity before and 30 min after injection of DREADD activator CNO (5 mg/kg i.p.) in mice expressing an inhibitory (left; 829 neurons, *** $p < 0.001$, Wilcoxon signed-rank test) or an excitatory (right; 411 neurons, *** $p < 0.001$, Wilcoxon signed-rank test) DREADD in SST interneurons.

(D) Average population mismatch responses of excitatory neurons before (green trace) and 30 min after (yellow trace) the injection of CNO in mice expressing an inhibitory DREADD in SST interneurons (4 mice, 829 neurons). Orange bar indicates duration of mismatch, shading indicates s.e.m. Statistical comparisons as in **Figure 1E**.

(E), Same as in (**D**), but for mice expressing an excitatory DREADD in SST interneurons (2 mice, 411 neurons).

Figure 6

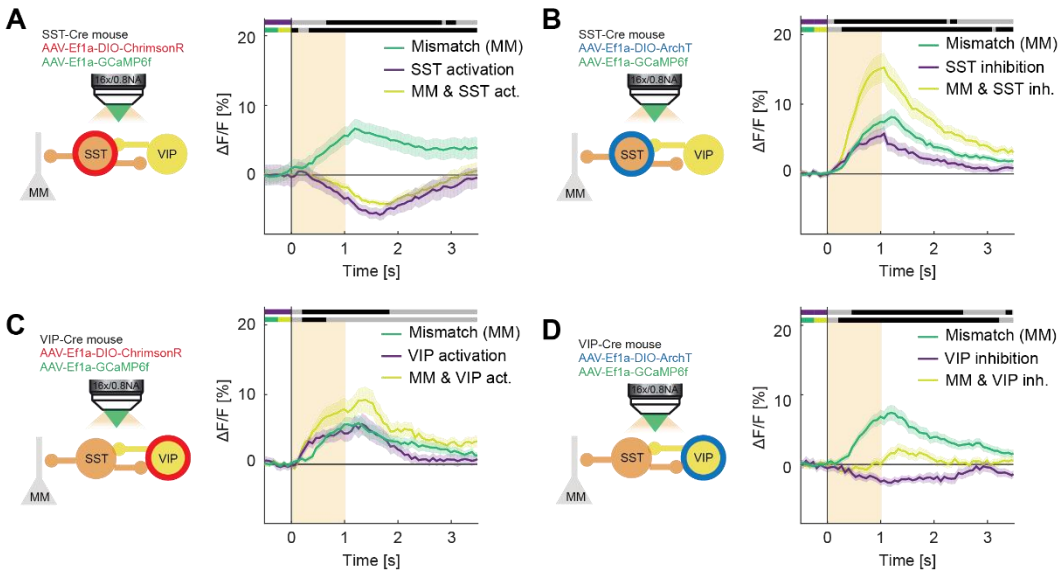

Figure 6. Mismatch neurons are inhibited by SST activation or VIP inhibition and activated by SST inhibition or VIP activation.

(A) Left: Schematic of the experimental design. ChrimsonR was selectively expressed in SST interneurons and GCaMP6f in all neurons. We then locally activated SST interneurons through the imaging objective while imaging GCaMP6f activity in all neurons. Right: Response of putative excitatory mismatch-responsive neurons (165 neurons, 5 mice) to mismatch (green line), optogenetic activation of SST interneurons during running (purple line), and concurrent mismatch and optogenetic activation of SST interneurons (yellow line). Orange area indicates duration of mismatch and duration of optogenetic stimulation respectively, shading indicates s.e.m. Statistical comparisons as in **Figure 1E,** but for 67 ms bins. Upper line marks comparison of manipulation-only against baseline, lower line marks comparison of mismatch only against concurrent mismatch and optogenetic stimulation.

(B) Left: As in (**A**), but expressing ArchT in SST interneurons. Right: Responses of mismatch neurons (236 neurons, 4 mice) as in (**A**), but for optogenetic inhibition of SST interneurons.

(C) Left: As in (**A**), but expressing ChrimsonR in VIP interneurons. Right: Responses of mismatch neurons (114 neurons, 4 mice) as in (**A**), but for optogenetic activation of VIP interneurons.

(D) Left: As in (**A**), but expressing ArchT in VIP interneurons. Right: Responses of mismatch neurons (107 neurons, 3 mice) as in (**A**), but for optogenetic inhibition of VIP interneurons.

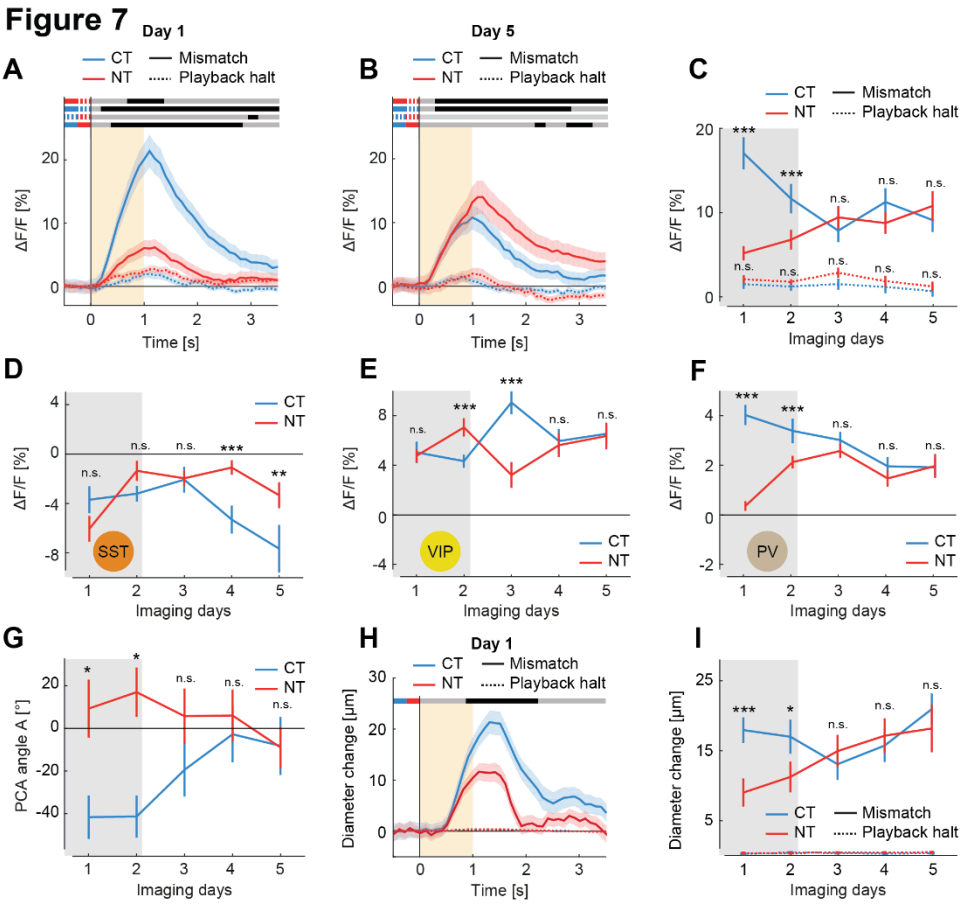

Figure 7. Normal visuomotor experience restores normal visuomotor integration.

(A) Average responses to mismatch (solid lines) and playback halt (dashed lines) of neurons with positive correlation of activity with running speed (running correlation greater than 0.05) and negative correlation of activity with visual flow (visual correlation smaller than -0.05) on the first imaging day (CT: 12% ± 2% of neurons per mouse, 9 mice; NT: 10% ± 3%, 9 mice). Orange area indicates duration of mismatch, shading indicates s.e.m. Statistical comparison as in **Figure 1E**.

(B) Same as (**A**), but for last imaging day (CT: 10% ± 2% of neurons per mouse, 8 mice; NT: 9% ± 1%, 7 mice).

(C) Average responses to mismatch and playback halt (see Methods) of excitatory neurons selected as in (**A**) as a function of imaging days for CT and NT mice. Mice were dark reared until the second imaging session (indicated by gray area). Error bars indicate s.e.m. *: $p < 0.05$, **: $p < 0.01$, ***: $p < 0.001$, n.s., not significant, $p \geq 0.05$, Mann-Whitney-U test.

(D) Average population responses to mismatch of SST interneurons, as a function of imaging days for CT and NT mice.

(E) As in (**D**) but for VIP interneurons.

(F) As in (**D**) but for PV interneurons.

(G) Mean angle of first principal component (as in **Figures 2B and 2C**; see Methods) relative to the y-axis for CT and NT mice as a function of imaging days. Gray area indicates dark rearing, error bars indicate s.e.m.

(H), Average pupil dilation in response to mismatch and playback halt for CT (25 mice) and NT mice (25 mice; see Methods) on the first imaging day. Orange area indicates duration of mismatch, shading indicates s.e.m. Statistical comparisons as in **Figure 1E**, but for $p<0.05$.

(I), Average pupil dilation in response to mismatch and playback halt a function of imaging days for CT and NT mice. Gray area indicates dark rearing, error bars indicate s.e.m. *: $p < 0.05$, **: $p < 0.01$, ***: $p < 0.001$, Mann-Whitney-U test.

Figure S1

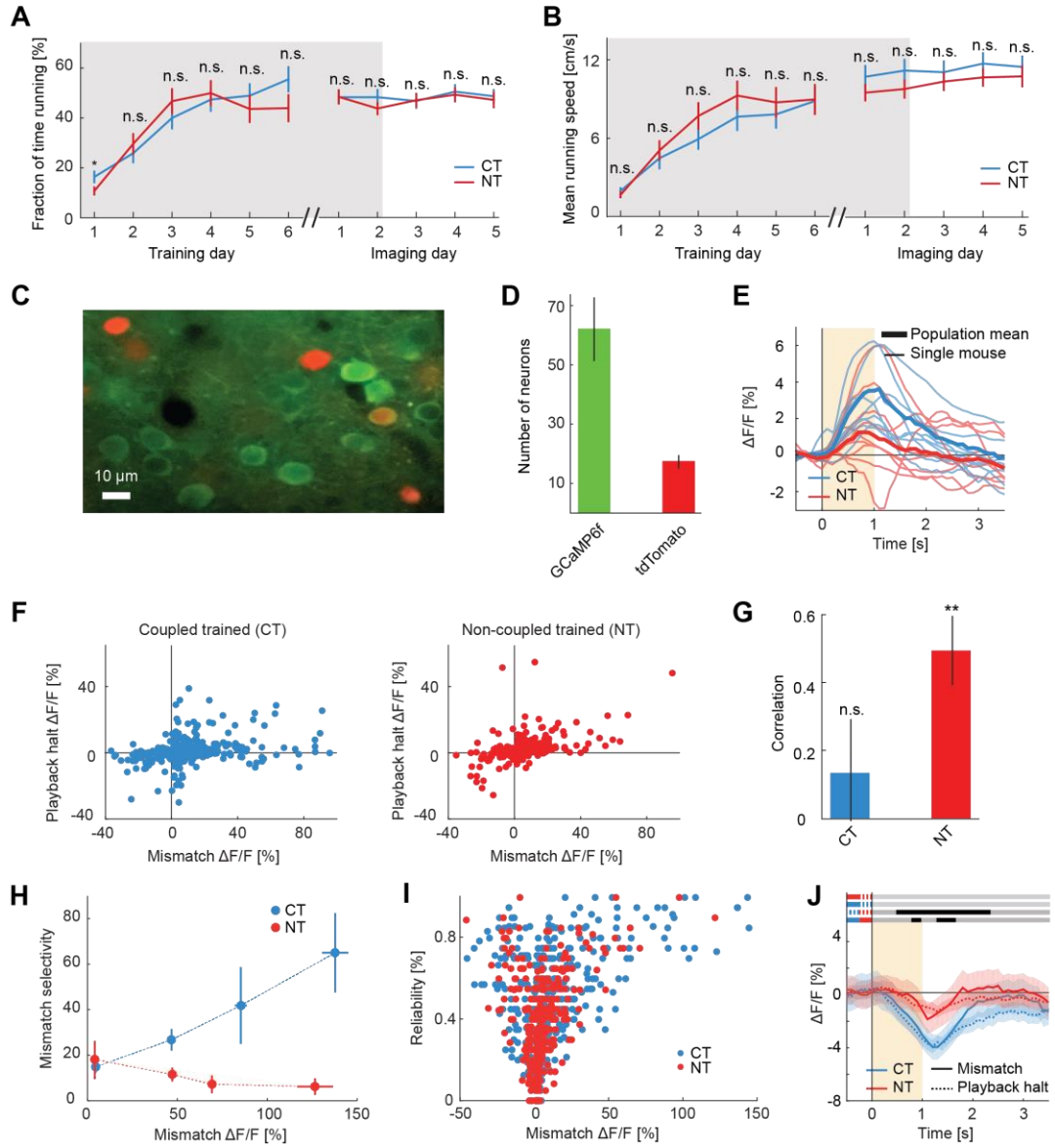

Figure S1. Analysis of running behavior, tdTomato expression, and additional analysis of mismatch and playback halt responses. Related to Figure 1.

(A) Fraction of time spent running increased during training period (left) for CT mice (36 mice) and NT mice (36 mice) and remained stable during imaging sessions (CT: 31 mice; NT: 30 mice). Error bars indicate s.e.m., gray shading indicates dark rearing. n.s., not significant, $p \geq 0.05$, Student's t test.

(B) Same as in (**A**), but for average running speed. Average running speed increased during training (left) and remained stable during imaging sessions (right). Error bars indicate s.e.m., gray shading indicates dark rearing.

(C) Two-photon image of layer 2/3 neurons in mouse V1. In vGAT-Cre x Ai14 mice, inhibitory interneurons express tdTomato and are shown in red. Expression of GCaMP6f (green) under the EF1α promoter resulted in 96.8% ± 0.7% (3321 of 3438 in total, mean ± s.e.m.) of GCaMP6f-positive neurons that were not tdTomato positive. The surprisingly small overlap between GCaMP6f and tdTomato expression may in part result from the selection bias of GCaMP6f-positive neurons towards active neurons.

(D) Number of GCaMP6f-expressing neurons and tdTomato-expressing neurons per field of view (375 µm x 300 µm; note that the example shown in (**C**) is not a full field of view; 7 mice). The ratio of GCaMP6f-expressing neurons to tdTomato-expressing neurons is approximately 3.5 across mice. If labeling were complete, and assuming that roughly 20% of neurons in cortex are interneurons (Markram et al., 2004), one would predict a ratio of 4.

(E) As in **Figure 1E**, but for individual mice. Average population response to mismatch in all CT (thin red lines) and NT (thin blue lines) mice. The mean response over all neurons of CT (NT) mice is the thick blue (red) line.

(F) Scatter plot of average mismatch and playback halt responses for CT mice (left; 865 neurons, 25 outside axis limits and not shown) and NT mice (right; 423 neurons, 3 outside axis limits and not shown) in excitatory neurons with significant response to mismatch (see Methods).

(G) Correlation between mismatch responses and playback halt responses for neurons with significant response to mismatch was significantly different from 0 in NT mice (9 mice, Student's t test, $p = 0.001$), but not in CT mice (9 mice, Student's t test, n.s., $p = 0.43$, see Methods). Error bars indicate s.e.m.

(H) Mismatch selectivity measured as the absolute ratio of the mismatch response to the playback halt response as a function of the mismatch response, in CT (blue) and NT mice (red). With increasing mismatch response, mismatch neurons in CT, but not NT, mice become increasingly selective for mismatch versus playback halt. Data are represented as mean plus s.e.m.

(I) Scatter plot for response reliability as a function of mismatch response for CT (blue; 865 neurons) and NT mice (red; 423 neurons) in excitatory neurons with significant responses to mismatch. Response reliability was calculated for each neuron as the fraction of mismatch events with a significant response (see Methods). Reliability was variable, but tended to increase with increasing mismatch responses.

(J) Average responses to mismatch (solid lines) and playback halt (dashed lines) of neurons with positive correlation of activity with visual flow (correlation greater than 0.05) on the first imaging

day (CT: 24% or 539 of 2259 of neurons, 9 mice; NT: 24% or 513 of 2104 neurons, 9 mice). Orange area indicates duration of mismatch, shading indicates s.e.m. Statistical comparison as in **Figure 1E.**

Figure S2

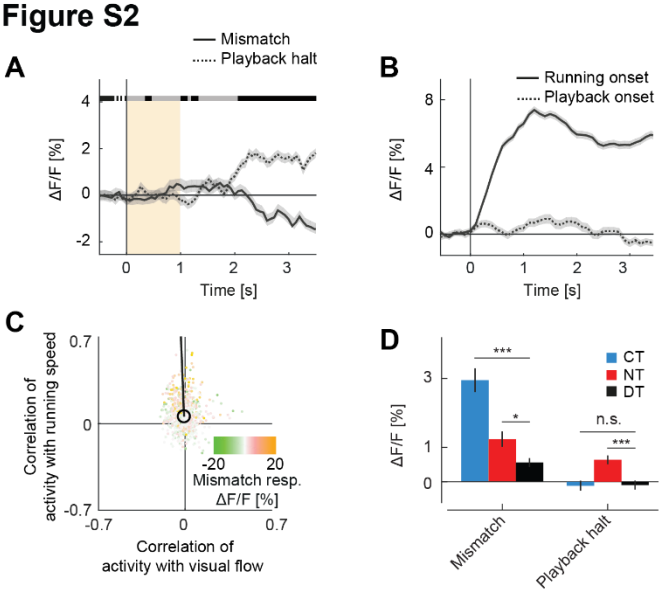

Figure S2. Population responses and correlation patterns in dark trained (DT) mice. Related to Figures 1 and 2.

(A) Average population responses to mismatch (solid line) and playback halt (dashed line) for excitatory neurons in DT mice (6 mice, 1076 neurons). Shading indicates s.e.m. Statistical comparisons as in **Figure 1E**, but for 67 ms time bins.

(B) Same as in (**A**), but for running onset in closed-loop session and playback onset in open-loop session.

(C) As in **Figure 2B**, but for DT mice. Correlation coefficients between neural activity (ΔF/F) of layer 2/3 excitatory neurons with running speed or with visual flow during open-loop sessions in DT mice. Each dot represents a single neuron. The color of each point indicates the amplitude of the mismatch response. The black circle marks mean correlation values. The solid black line indicates the angle of the mean first principle component of the distribution (see Methods).

(**D**) Comparison of mismatch responses and playback halt responses of CT, NT and DT mice. *: $p < 0.05$, ***: $p < 0.001$, Student's t test.

Figure S3

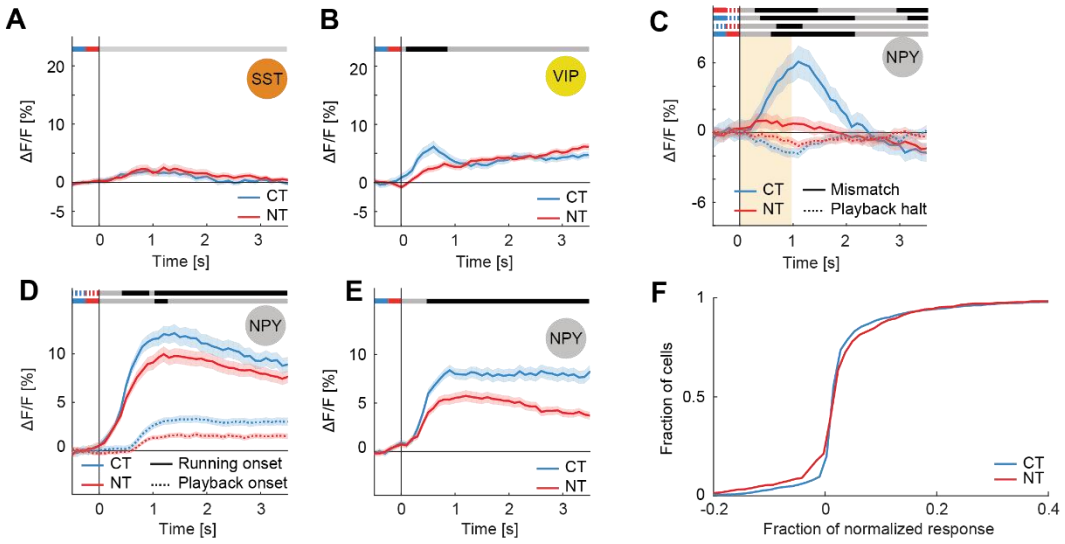

Figure S3. Additional analysis of interneuron responses. Related to Figure 4.

(A and B), Running-onset responses in complete darkness for SST (**A;** CT: 5 mice, 118 neurons; NT: 5 mice, 157 neurons) and VIP (**B**; CT: 3 mice, 189 neurons; NT: 3 mice, 137 neurons) interneurons on first imaging day. Statistical comparisons as in **Figure 1E**.

(C) Average population responses to mismatch (solid line) and playback halt (dashed line) for NPY interneurons from CT (9 mice, 456 neurons) and NT (7 mice, 445 neurons) mice on first imaging day. Orange area indicates duration of mismatch, shading indicates s.e.m. Statistical comparisons as in **Figure 1E**.

(D) Same as in (**C**), but for running-onset responses in closed-loop sessions (solid lines) and playback onset in open-loop sessions (dashed lines) on first imaging day. Statistical comparison as in **Figure 1E**.

(E) Same as in (**D**), but for running-onset responses in complete darkness on first imaging day. Statistical comparison as in **Figure 1E**.

(F) Cumulative density plot of normalized mismatch responses of excitatory mismatch responsive neurons for CT (2259 neurons) and NT (2104 neurons) mice on first imaging day. Note the response distribution of the NT neurons is wider than that for CT neurons ($p < 0.01$, Kolmogorov–Smirnov test). This indicates that the distribution of mismatch responses over neurons is sharpened in CT mice, potentially by the selective activation of PV interneurons (**Figure 4E**).

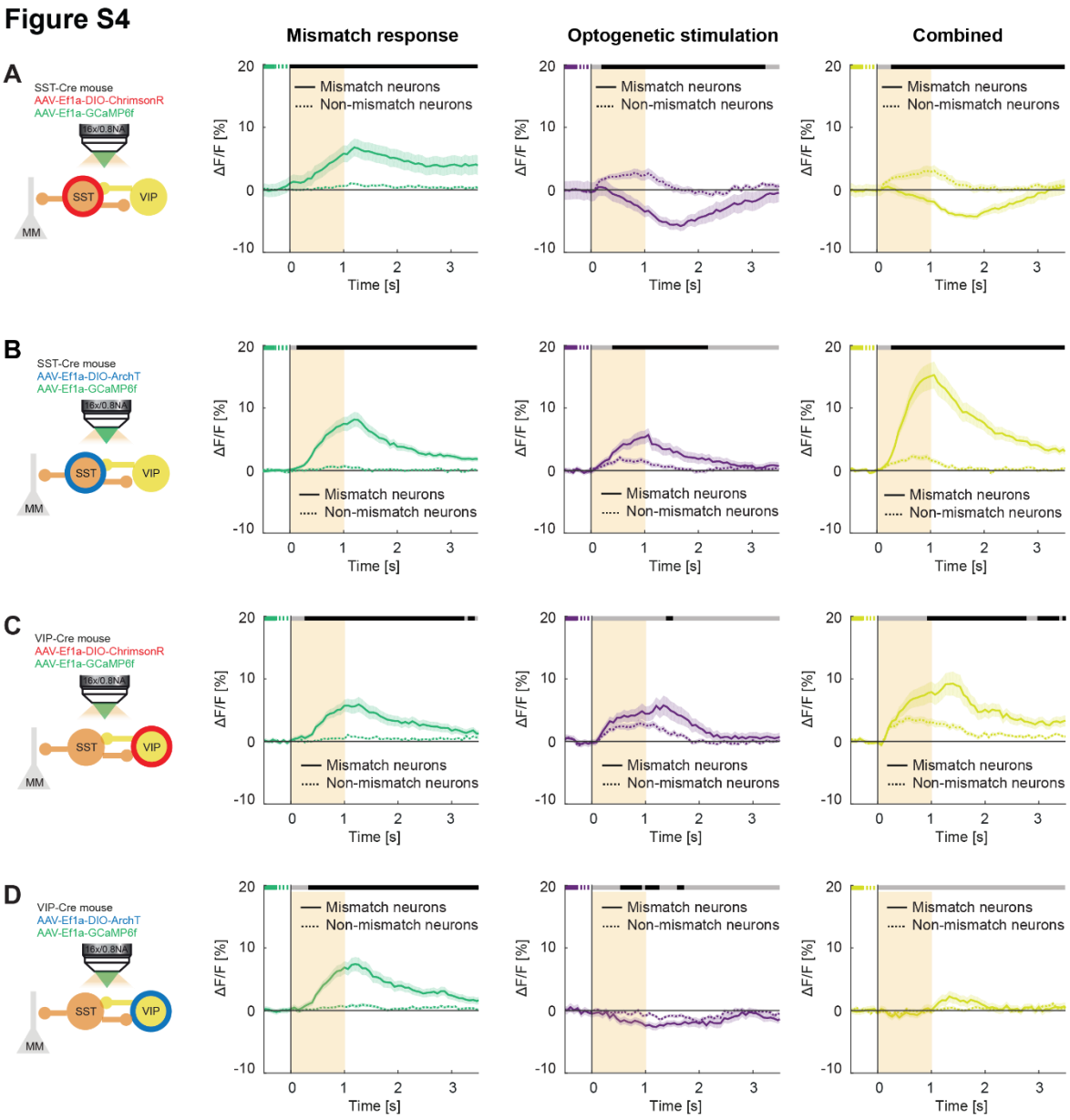

Figure S4. A subset of excitatory neurons decrease activity during mismatch. Related to Figure 6.

(A) Left: Average responses to mismatch of 20% of neurons with the largest, positive mismatch response (solid green line, 165 neurons, 4 mice, the same neurons shown in **Figure 6**) and of 20% of neurons with no mismatch response (dashed green line, 165 neurons). Middle: Average response of the same mismatch responsive (solid purple line) and non-mismatch responsive neurons (dashed purple line) to optogenetic activation of SST interneurons. Right: Average response of mismatch responsive (solid yellow line) and non-mismatch responsive neurons (dashed yellow line) to concurrent optogenetic activation of SST interneurons and mismatch. Orange area indicates duration of mismatch and duration of optogenetic stimulation, shading indicates s.e.m. Statistical comparison as in **Figure 1E**, but for 67 ms time bins.

(B) As in (**A**), but for optogenetic inhibition of SST interneurons (236 neurons in each group, 4 mice).

(C) As in (**A**), but for optogenetic activation of VIP interneurons (114 neurons in each group, 4 mice).

(D) As in (**A**), but for optogenetic inhibition of VIP interneurons (107 neurons in each group, 3 mice).

Figure S5

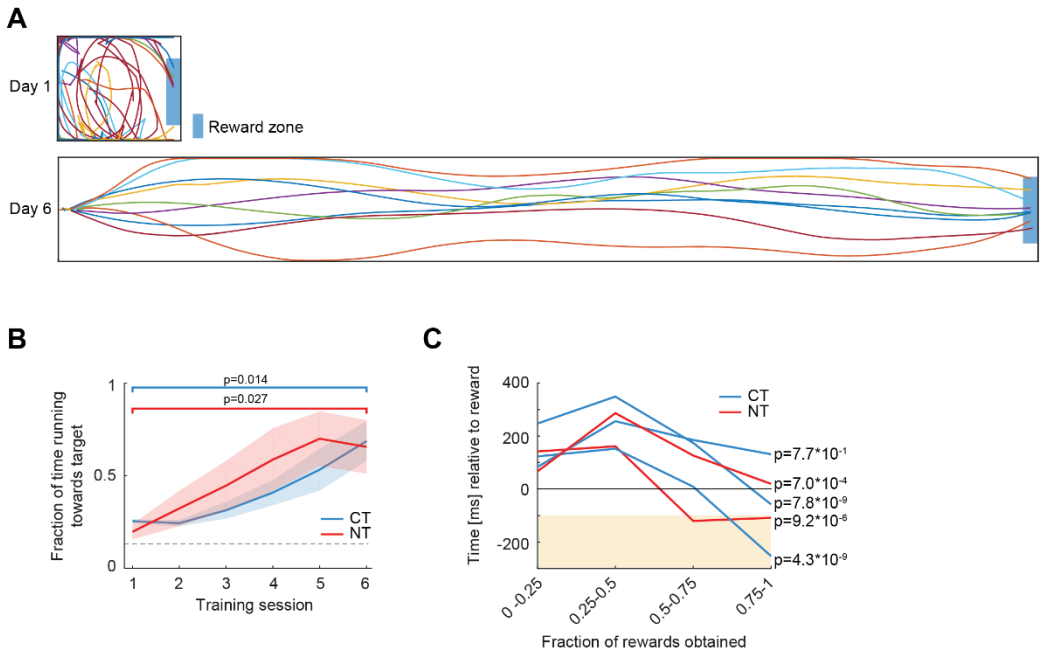

Figure S5. Both CT and NT mice learn to perform visuomotor tasks. Related to Figure 7.

(A) In a two-dimensional (2D) virtual locomotion task, water restricted mice need to learn to control a freely rotating styrofoam ball in order to traverse a linear corridor and reach a reward zone (blue shaded area). The length of the corridor was automatically increased as performance increased to keep reward rate constant. Upper panel: Sample trajectories of a single mouse in the 2D virtual environment on day 1. Trajectories were random, however the tunnel was short (approximately 0.5 m) and mice obtained rewards by chance. Once a reward was obtained, the mouse was teleported back to the beginning of the tunnel after a brief timeout (2 s) to start the next trial. Lower panel: Sample trajectories of the same mouse as in upper panel, but on day 6 when the mouse had learned the task (tunnel length approximately 6 m).

(B) Both CT (6 mice) and NT mice (4 mice) learned the 2D virtual locomotion task over the course of 6 training sessions (1 h/day). Task performance was quantified as the fraction of time spent running towards the reward zone. There was a significant increase from training session 1 to training session 6 for CT and NT mice (Student's t test). Shading indicates s.e.m.

(C) In a mismatch detection task, mismatch is followed by a water reward (100 ms delay after end of mismatch). Behavior is quantified as the latency to the first lick relative to the water reward (see Methods). Mice were water restricted and habituated to licking from the water spout prior to testing. In the first training sessions, mice only licked after reward delivery. Over the course of 3 to 5 training sessions (1 h per day), both NT (n = 2) and CT (n = 3) mice started to lick during mismatch,

before the reward was delivered. Orange area indicates mismatch. Shown is the mean time to the first lick as a function of the fraction of rewards obtained throughout training. To assess learning, we compared the distribution of the lick times of the first training session to the last training session for each mouse (sided Mann-Whitney-U test, p-values indicated adjacent to learning curve).

Figure S6

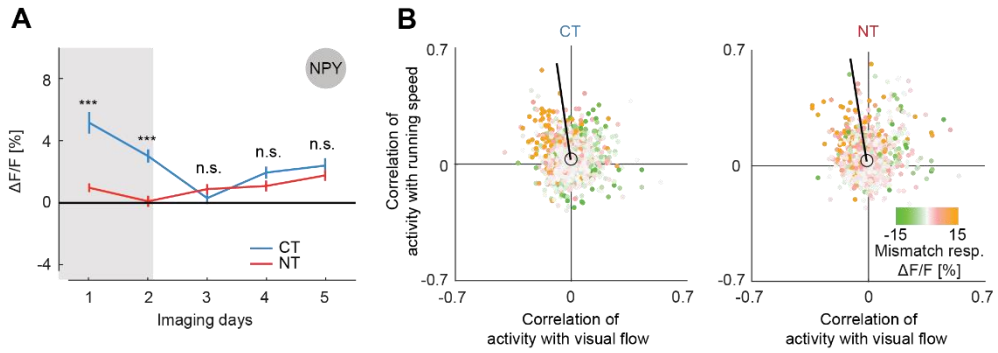

Figure S6. Normal visuomotor experience equalizes mismatch responses in NPY interneurons and correlation patterns in excitatory neurons. Related to Figure 7.

(A) Mismatch responses of NPY interneurons averaged over a 1 s window (see Methods) as a function of imaging days for CT and NT mice. Mice were dark reared until the second imaging session (indicated by gray area). Error bars indicate s.e.m. *: $p < 0.05$, **: $p < 0.01$, ***: $p < 0.001$, Mann-Whitney-U test.

(B) Correlation coefficients between neural activity (ΔF/F) and running speed or visual flow in CT (left) and NT (right) mice during open-loop sessions on imaging day 5. Each dot represents a single neuron (CT: 8 mice, 2213 neurons; NT: 7 mice, 1686 neurons). Dot color indicates the neuron's mismatch response. Black circles indicate mean correlations. Solid black lines indicate mean angle of first principle component of the distributions for each mouse (see Methods).

Figure S7

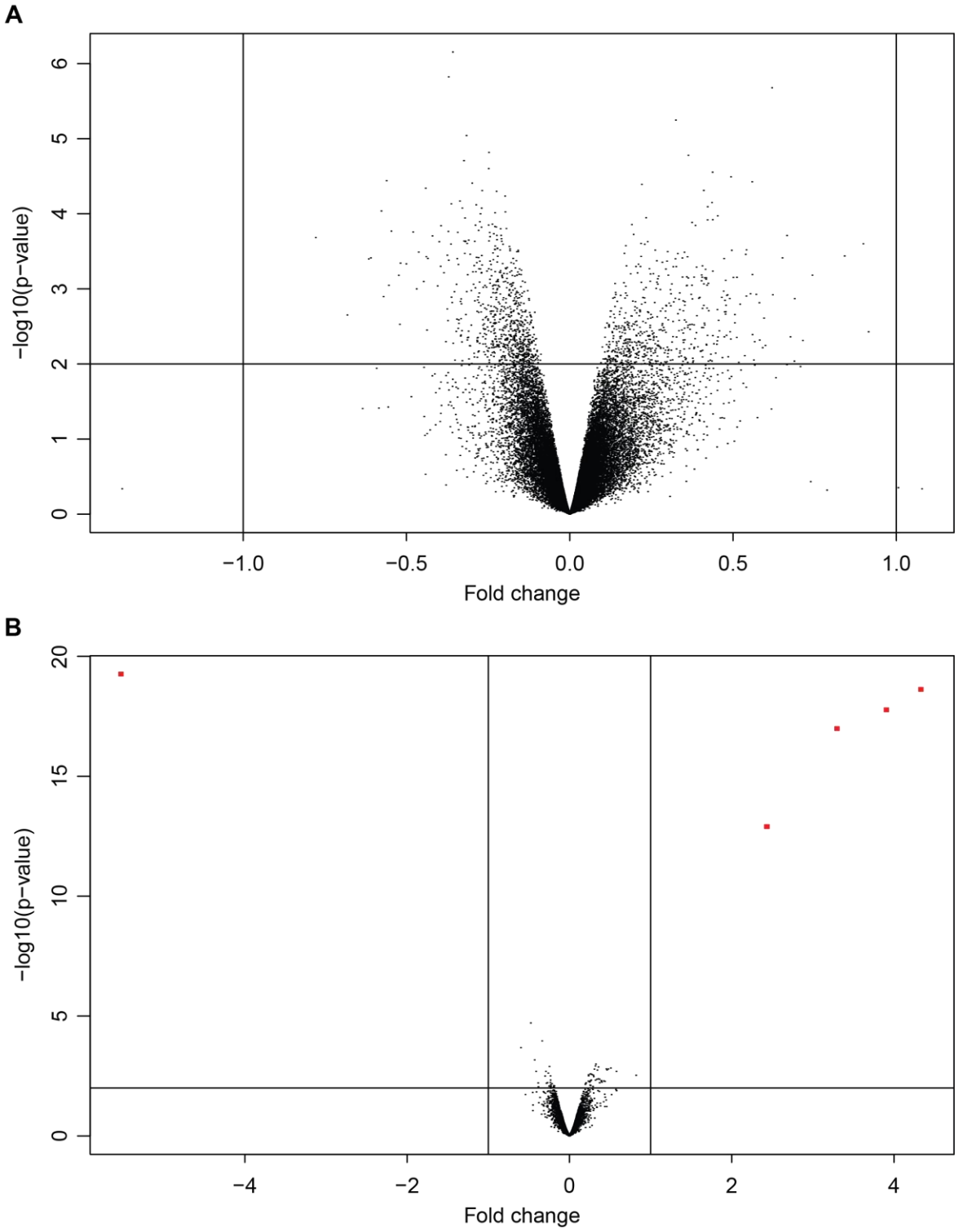

Figure S7. Volcano plots highlighting genes with significant fold changes when comparing between CT and NT animals **(A)** or comparing between male and female animals **(B)**.Cutoff thresholds are p < 0.01 and two-folds.

Table S1

	2nd session			5th session		
	Safe	Cliff	Safe%	Safe	Cliff	Safe%
CT1	6	4	60%	2	1	67%
NT1	3	5	38%	0	0	-
CT2	3	0	100%	0	0	-
NT2	6	0	100%	6	1	86%
CT3	4	2	67%	1	0	100%
NT3	1	0	100%	0	0	-
CT total	13	6	68%	3	1	75%
NT total	10	5	67%	6	1	86%
Controls	6	0	100%	-	-	-

Table S1. Results of visual cliff tests for CT and NT animals after the second imaging session and after the 5th imaging session. Number of choices made on the safe or cliff side are listed, with percentage of choosing safe over the total number of choices. Data from controls animals are from a few different normal-reared animals.

Table S2

Gene ID	Gene Name	Gene Description	mRNA ID
NR_001463	Xist	inactive X specific transcripts	NR_001463
NM_011419	Kdm5d	lysine (K)-specific demethylase 5D	NM_011419
NM_012011	Eif2s3y	eukaryotic translation initiation factor 2, subunit 3, structural gene Y-linked	NM_012011
NM_009484	Uty	ubiquitously transcribed tetratricopeptide repeat gene, Y chromosome	NM_009484
NM_012008	Ddx3y	DEAD (Asp-Glu-Ala-Asp) box polypeptide 3, Y-linked	NM_012008

Table S2. Genes that appeared as with significant fold changes in **Figure S7B**.

Methods[2]

Animals and surgery. All animal procedures were approved by and carried out in accordance with guidelines of the Veterinary Department of the Canton Basel-Stadt, Switzerland. Six different mouse lines were used in the present study: wild-type C57BL/6J mice, vGAT-Cre x Ai14 tdTomato mice, PV-Cre ($Pvalb^{tm1(cre)Arbr}$) (Hippenmeyer et al., 2005), SST-Cre ($Sst^{tm2.1(cre)Zjh}$) (Taniguchi et al., 2011), VIP-Cre ($Vip^{tm1(cre)Zjh}$) (Taniguchi et al., 2011) and NPY-Cre ($Npy^{RH26Gsat/Mmucd}$) (Gerfen et al., 2013) mice. Mice were dark-reared from birth (except mice used for pharmacogenetic manipulation experiments) and weaned on postnatal day 21 (P21). On P30, mice were briefly anesthetized with isoflurane in the dark and then received a subcutaneous injection of a Fentanyl (0.05 mg/kg; Actavis), Midazolam (5.0 mg/kg; Dormicum, Roche) and Medetomidine (0.5 mg/kg; Domitor, Orion) mixture. A 4 mm craniotomy was made over the right V1, centered on 2.5 mm lateral and 1 mm anterior of lambda. We labelled neurons with a calcium indicator by injecting an AAV2/1 vector (see section "Viral constructs" below for details) into right monocular V1, centered on 2.5 mm lateral and 0.5 mm anterior of lambda (3-4 injections per mouse, approx. 100-150 nl per injection). A 4 mm circular cover glass was glued in place using gel superglue (Ultra Gel, Pattex). The remaining exposed surface of the skull was scored with a needle to increase adhesion with glue and dental cement, and covered with Histoacryl (B. Braun). A titanium head bar was fixed to the skull using dental cement (Paladur, Heraeus Kulzer) (Leinweber et al., 2014). Mice were returned to their home cage in darkness after anesthesia was antagonized by an intraperitoneal injection of a Flumazenil (0.5 mg/kg; Anexate, Roche) and Atipamezole (2.5 mg/kg; Antisedan, Orion Pharma) mixture.

DREADD and optogenetic experiments. We used 7 to 16 weeks old male and female SST-Cre mice (for DREADD and optogenetic experiments) and VIP-Cre mice (for optogenetic experiments) that were reared in normal conditions. Craniotomy, virus injection, and headbar fixation was performed as described above. Mice were habituated to the setup 9 days post surgery. Imaging experiments started 2 weeks post surgery.

Viral constructs. We used AAV2/1-EF1α-GCaMP5 (titer: $3.4 * 10^{11}$ GC/ml) for wild-type, EF1α-CGaMP6f (titer: $5.6 * 10^{11}$ - $4.4 * 10^{12}$ GC/ml) for vGAT-Cre x Ai14, pharmacogenetic, and optogenetic experiments, and EF1α-DIO-GCaMP6f (titer: $3.0 * 10^{11}$ - 7.8×10^{11} GC/ml) for inhibitory interneuron marker lines. To manipulate neural activity pharmacogenetically, we injected AAV2/1-EF1α-DIO-hM4D(Gi)-mCherry (titer: $7.0 * 10^{11}$ GC/ml) or AAV2/1-EF1α-DIO-hM3D(Gq)-mCherry (titer: $3.4 * 10^{11}$ GC/ml). For optogenetic manipulations of SST and VIP interneuron activity, we

[2] Most of the Methods section also appear in the manuscript of the paper which has been submitted to Cell, with modifications.

injected AAV2/1-EF1α-DIO-ChrimsonR-tdTomato (titer: 2.2 * 10^{11} GC/ml) or AAV1-CAG-FLEX-ArchT-tdTomato (titer: 3.1 * 10^{12} GC/ml).

We initially attempted to label Cre-positive interneurons by means of a floxed RFP virus (AAV2/1-EF1α-DIO-tdTomato) and bulk label all neurons with an unconditional GCaMP6f (AAV2/1- EF1α-GCaMP6f) to concurrently record the activity of the selected interneuron type and all other neurons. However, for reasons unclear to us, this led to a very low co-labeling yield and signals in interneurons were often contaminated by the much stronger signals in surrounding excitatory neurons. We speculate that the reason for this may be that the promoter used (EF1α) to drive the GCaMP6f expression is stronger in excitatory neurons than interneurons.

Virtual reality environment setup. The setup is based on the design of Dombeck and colleagues (Dombeck et al., 2007). Briefly, mice were head-fixed and free to run on an air-supported spherical treadmill. Rotation of the ball was restricted around the vertical axis with a pin. The virtual reality environment was projected onto a toroidal screen covering approximately 240 degrees horizontally and 100 degrees vertically of the mouse's visual field using a projector (Samsung SP-F10M) synchronized to the resonant scanner of the two-photon microscope. The virtual environment consisted of an infinite corridor with walls patterned with vertical sinusoidal gratings with a spatial frequency of approximately 0.04 cycles per degree (Leinweber et al., 2014).

Two-photon imaging. Functional two-photon calcium imaging was performed using 2 custom-built two-photon microscopes (Leinweber et al., 2014). Illumination source was a tunable femtosecond laser (Insight, Spectra Physics; Coherent Chameleon) tuned to 990 nm. Emission light was band-pass filtered using a 525/50 filter for GCaMP and a 607/70 filter for tdTomato/mCherry (Semrock) and detected using a GaAsP photomultiplier (H7422, Hamamatsu). Photomultiplier signals were amplified (DHPCA-100, Femto), digitized (NI5772, National Instruments) at 800 MHz, and band-pass filtered around 80 MHz using a digital Fourier-transform filter implemented in custom-written software on an FPGA (NI5772, National Instruments). The scanning system of the microscopes was based either on a 12 kHz or an 8 kHz resonant scanner (Cambridge Technology). Images were acquired at a resolution of 750 x 400 pixels (60 Hz / 40 Hz frame rate, respectively), and a piezo-electric linear actuator (P-726, Physik Instrumente) was used to move the objective (Nikon 16x, 0.8 NA) in steps of 15 µm between frames to acquire images at 4 different depths. This resulted in an effective frame rate of 15 Hz or 10 Hz, respectively. The field of view was 375 µm x 300 µm.

Simultaneous two-photon imaging and optogenetic stimulations. ChrimsonR or ArchT stimulation and functional imaging of GCaMP6f-expressing neurons was done by using a modified Thorlabs B-Scope with a 12 kHz resonance scanner (Cambridge Technology) for line scanning. Illumination

source for the optogenetic stimulation was a fast LED (UHP-T-595, Prizmatix) with a wavelength of 595 nm and which allowed fast TTL triggered operation. For spectral filtering we used a dichroic mirror (ZT775sp-2p, Chroma) to combine the two-photon laser and stimulation light. A second long-pass dichroic mirror (F38-555SG, Semrock) was used to split the GFP emission from both illumination light sources. Light leak from the 595 nm stimulation LED was reduced by synchronizing the LED light output to the turnaround times of the resonant scanner (during which imaging data were not acquired). Lastly, amplified PMT signals were digitally bandpass filtered at 80 MHz to reduce the effect of ringing in the amplifier. This allowed for near stimulation-artifact free synchronous imaging and optogenetic stimulation.

Experimental design. Mice were kept in the dark for an additional 2 days following surgery, after which they were introduced to the virtual reality environment. Mice were briefly anesthetized with isoflurane in the dark and then head-fixed on the setup. CT and NT mice were trained in pairs. The visual flow projected onto both screens was coupled to the locomotion of the CT mouse (**Figure 1B**). For dark training, mice were head-fixed and trained on the setup in complete darkness. All mice were free to run on the ball throughout training. In total, all CT, NT, and DT mice underwent 6 training sessions of 2 hours every other day (**Figure 1A**).

The first imaging experiment was performed 2 days after the last training session. The design of the imaging experiments was as previously described (Keller et al., 2012). Typically, an imaging experiment consisted of 1 closed-loop session and 2 open-loop sessions. In closed-loop sessions, the visual flow was coupled to the locomotion of the mouse, and was randomly perturbed with brief (1 s) halts (mismatch; one perturbation every 15 seconds on average). In open-loop sessions, the visual flow generated in the closed-loop session (including perturbations, here referred to as playback halt) was replayed to the mouse independent of its locomotion. For some mice, open-loop sessions were followed by a dark session, where the virtual reality and all other light sources in the room were turned off. Each closed-loop, open-loop or dark session lasted 500 s. To minimize the effect of altered visuomotor experience (non-coupled experience in open-loop sessions for CT mice, and vice versa), we controlled the visual stimuli between imaging sessions so as to be the same as they were experienced in the training sessions, such that CT mice experienced closed-loop conditions (no perturbations) and NT and DT mice experienced open-loop conditions. Mice were kept in darkness between training and imaging sessions until after the second imaging session at which point they were transferred to in a normal 12 h/12 h light/dark cycle (**Figure 1A**). Note that DT mice were only imaged on time points 1 and 2.

At the end of each experiment intrinsic optical imaging was performed as described previously (Zmarz and Keller, 2016) to verify that the retinotopic location of recording sites corresponded to a part of the visual field covered by the toroidal screen.

Two-photon imaging data analysis. Calcium imaging data were processed as previously described (Keller et al., 2012) and all data analysis was done in MATLAB (MathWorks). Briefly, raw images were full-frame registered to correct for brain motion. Neurons were manually selected based on mean and maximum fluorescence images. Raw fluorescence traces were corrected for slow drift in fluorescence using an 8th-percentile filtering with a 15 s window (Dombeck et al., 2007). ΔF/F traces were calculated as mean fluorescence in a selected region of every imaging frame and subsequently subtracted and normalized by the median fluorescence.

To quantify average response traces, we first calculated the average event-triggered fluorescence trace for each neuron. The responses of all neurons were then averaged and the baseline (mean ΔF/F in a 0.5 s window pre event onset) was subtracted. To quantify the significance of the difference of two average calcium responses as a function of time, we performed a separate Student's t test for every bin of the calcium trace (10 Hz or 15 Hz) and marked bins as significantly different for $p < 0.01$. For visual clarity, we removed isolated significant bins, such that a significant bin was only marked if at least one of the two neighboring bins was also significant.

To calculate the average response of each neuron to mismatch or playback halt, we first calculated the difference between the average event-triggered response and the average response to 1000 randomly triggered events to generate a random-corrected trace. Average responses to mismatch and playback halt were then calculated as the mean fluorescence of the random-corrected average in a response window minus the mean fluorescence in a baseline window for each neuron (the response window for mismatch, playback halt, running onset and playback onset was +500 ms to +1500 ms, and the baseline subtraction window was -1000 ms to 0 ms). To determine the significance of a neuron's response, we calculated individual neuron responses to each mismatch event as described above and compared this distribution to the distribution generated by 1000 randomly triggered events. Significance was determined with a two sided Mann-Whitney-U test ($p < 0.05$). For mismatch and random events to be included in the analysis, mice had to be running above threshold (10^{-2} cm/s) before and after event onset (from -600 ms to + 1100 ms). In addition, for playback halt events to be included, mice had to be stationary during the playback halt (no running from -600 ms to +1100 ms). For running onset, mice had to be stationary for at least 600 ms prior to the running onset and continue running for 1100 ms above threshold following the onset. Similarly, for playback onset (quantified only during open-loop sessions) there had to be no visual flow for 600

ms prior to visual flow onset, followed by continuous visual flow above threshold for at least 1100 ms after onset, mice had to be stationary during this time.

To determine correlation between mismatch responses and playback halt responses (**Figures S1F and S1G**), we calculated Pearson's linear correlation coefficients for each mouse between the vector containing the mismatch responses of all neurons and the vector containing the playback halt responses for each neuron.

We calculated Pearson's linear correlation coefficients to determine the correlation between individual neural activity and visual flow or running speed during the open-loop sessions. To minimize the influence of running-induced z-motion on the correlation coefficients, we calculated a threshold for each neuron (3.72 * standard deviation of the lower half of the fluorescence distribution) (Keller et al., 2012) and set all activity below this threshold to 1 (note that for ΔF/F, baseline is at 1). To calculate the average correlations over days (**Figure 3**), we first calculated the average correlations per day and then averaged these across all imaging time points.

To calculate the principal component of the correlation distributions, we used the standard implementation available in MATLAB. We calculated the principal component for each imaging region separately. To calculate the average angle, we averaged the vector sum of the normalized principle components of all imaging regions.

We calculated the average traces for the optogenetic experiments (**Figures 6, S4**), as described above. To further reduce the stimulation artefact after filtering, we used the following approach. The remaining stimulation artifact was approximated as a box function and subtracted from the average stimulation response of each neuron. The amplitude of the box function was estimated as the average of the of the absolute difference between the calcium signal on frame n-1 and n, and m and m+1, where the stimulation light was switched on between frame n-1 and n and switched off between m and m+1. On average this signal was 0.8% dF/F and much smaller than the typical neural response (**Figure 6 and S4**).

Average running speed during training and imaging sessions was calculated as the mean speed while the mouse was running above threshold (10^{-2} cm/s). Fraction of time running during training and imaging sessions was calculated as the fraction of time running speed was above threshold (10^{-2} cm/s) over total session duration. Note that during imaging sessions, fraction of time spent running and average running speed were calculated on the combined closed-loop and open-loop sessions.

Pupil dilation. Images of the left eye, contralateral to the craniotomy, were recorded with a CMOS camera at 30 Hz (DMKBUC03, Imaging Source). Pupil position was computed offline by smoothing

and thresholding the images and fitting a circle to the pupil. Data containing eye blinks were excluded from analysis. To extract mismatch induced pupil diameter changes, we computed the difference between the average dilation triggered on mismatch and the average dilation triggered on 1000 randomly chosen onsets. Average responses to mismatch was calculated as the difference between the amplitude averaged over a window pre (-100 ms to 0 ms) and post (+500 ms to +1500 ms) mismatch on the random-subtracted traces. To quantify significant difference as a function of time, we used the same bin-by-bin comparison described for calcium responses above, but with black bars indicating $p < 0.05$.

To determine neural response times, we calculated the time point of significant deviation between mismatch response traces of neurons with significant response to mismatch and randomly triggered traces (see above). For each neuron, we compared the fluorescence distributions of mismatch responses to random responses for each frame after the event onset (from 0 ms to +1500 ms). The response time was then taken as the first frame where the two distributions were significantly different (Mann-Whitney-U test, $p < 0.05$). The response time was only scored if the response distributions at 0 ms were not different and the responses diverged within the time window. This was the case for all excitatory neurons with significant response to mismatch. Pupil response times were calculated similarly.

Mismatch detection paradigm and 2D virtual locomotion task. Mice were dark-reared from birth and trained as either CT or NT, as described above. After the last training session, the water bottle was removed from the home cage. The weight of the mice was monitored throughout behavioral training and water was supplemented if necessary to keep the weight above 80% of initial weight. Mice were habituated to the lick spout in 2 sessions (1 h each). Experiments started 2 days after the last training session. For the mismatch detection paradigm, we put the mice into the same virtual reality environment as described above in a closed-loop configuration including visual perturbations (mismatch) as described above. A droplet (approx. 10 µl) of sucrose solution (15% in water) was delivered 100 ms after a mismatch via a metal spout placed in front of the mouse's snout. As mice learned the task, we observed anticipatory licking, which manifested as mice starting to lick during the 1 s mismatch, prior to reward delivery. A single experiment consisted of a 1 h closed-loop session during which the mice received approximately 100 rewards for a total of approximately 1 ml of sucrose solution. To assess learning for each mouse, the distribution of lick response times from the first training day was compared to the distribution of lick response times to the last training day using a Mann-Whitney-U test.

For the 2D virtual locomotion task, mice had to learn to navigate a virtual tunnel towards to a reward area marked by a blue cylinder. The rotation of the ball was not restricted and mice had to learn to control heading in the virtual tunnel via rotation of the ball. When a mouse reached the reward area, a droplet (approx. 10 µl) of sucrose solution (15% in water) was delivered via a lick spout. After a brief timeout (2 s), the position of the mouse in the virtual reality was reset to the starting location. The virtual tunnel was kept very short initially and the tunnel length was increased progressively as mice learned the task, such that the average number of rewards received per minute was held approximately constant (at 1.3 rewards per min). The behavior was quantified as the amount of time the mice spent running in the direction of the reward area (± 36° from reward-area direction), as a fraction of total time spent running. To quantify learning, the fraction of time spent running towards the target during training session 1 was compared to the fraction of time spent running towards the target on the last session for each mouse using a Student's t test.

Visual cliff test. The visual cliff apparatus consists of a piece of transparent glass (85 x 58 x 0.86 cm) surrounded by a 30 cm high wall made from white card paper to form an open top box. Half of the box was placed on the bench with another half suspended about 1 m above the floor. A piece of checkerboard cloth was placed between the glass and the bench and extended off the bench to the ground, highlighting the visual depth of the cliff. A black ridge (58 x 3 x 3 cm) was placed on the glass at the position of the bench edge, dividing the arena into a "shallow" and "deep" side. A lamp was placed under the glass to illuminate the apparatus and make the glass surface invisible. Each mouse was lifted with its tail and lowered onto the ridge, and waited until the mouse step off the ridge with all four paws on either side of the arena. Mouse which not steps off in 5 minutes will be counted as time out. The choice of the mouse will be recorded. Then the mouse was taken out of the apparatus and the procedure will be repeated up to ten times for each mouse.

Gene profiling. Wild-type C57BL/6J mice were dark-reared, and had head bar fixation surgeries on P26-30, as described earlier. For the first batch of mice, they were put in the virtual reality environment with either coupled or non-coupled training for a single session lasted six hours on P29-31; for the second batch of mice, they underwent three training sessions on three consecutive days, each session lasted for two hours. Mice were euthanized immediately after training, and bilateral visual cortices were dissected on ice for each mouse. RNAs were extracted using TRIzol Reagent (Life Technologies) and purified with RNeasy Mini Kit (QIAGEN), following procedures provided on the product manuals. RNA samples were then quantified with Nanodrop 1000 (ThermoFisher) and verified integrity with Bioanalyzer, and submitted to the FMI Functional Genomics platform for gene expression profiling with GeneChip microarray system (Affymetrix). Data are normalized and analyzed with linear models (limma) on a FMI hosted Galaxy server.

Acknowledgements

After I did my master's study on learning and memory, I became interested in how the brain encodes information and how computations are performed in neural circuits. This rather vague idea led me to apply for a PhD in the Keller lab at the FMI, and I was happy to have made the decision after the interview, as I found the tech-savvy feeling of the lab appealing. It turned out to be a very good choice, not only because I am fascinated by the idea of predictive coding, but also its intriguing implications on the mechanisms of psychiatric disorders, and not to mention the great environment in the lab and the whole FMI.

I would like to thank Georg Keller. I deeply appreciate the opportunity for pursuing my PhD, the wonderful environment of the lab, as well as all the help and support with both science and life alike. I admire his open attitude on science and learned a lot from him.

I would also like to thank people in the Keller lab for all the help during my PhD, especially Alex Attinger with whom I did most of the work in this study, as a reliable and friendly colleague; Daniela Gerosa for producing the AAV vectors; Marcus Leinweber for helping with building the microscope and programming; and Pawel Zmarz and Aris Fiser for all the good times we spent together.

Many thanks to Tom Mrsic-Flogel and Richard Hahnloser, the members of my PhD thesis committee for all the helpful discussions and comments on the project.

Last but not least, thanks to my parents for the support and all of my friends for being a part of my life and make it fun and enjoyable.

References

Adesnik, H., Bruns, W., Taniguchi, H., Huang, Z.J., Scanziani, M., 2012. A neural circuit for spatial summation in visual cortex. Nature 490, 226–31. doi:10.1038/nature11526

Akerboom, J., Chen, T.-W., Wardill, T.J., Tian, L., Marvin, J.S., Mutlu, S., Calderón, N.C., Esposti, F., Borghuis, B.G., Sun, X.R., Gordus, A., Orger, M.B., Portugues, R., Engert, F., Macklin, J.J., Filosa, A., Aggarwal, A., Kerr, R. a, Takagi, R., Kracun, S., Shigetomi, E., Khakh, B.S., Baier, H., Lagnado, L., Wang, S.S.-H., Bargmann, C.I., Kimmel, B.E., Jayaraman, V., Svoboda, K., Kim, D.S., Schreiter, E.R., Looger, L.L., 2012. Optimization of a GCaMP calcium indicator for neural activity imaging. J. Neurosci. 32, 13819–40. doi:10.1523/JNEUROSCI.2601-12.2012

Armbruster, B.N., Li, X., Pausch, M.H., Herlitze, S., Roth, B.L., 2007. Evolving the lock to fit the key to create a family of G protein-coupled receptors potently activated by an inert ligand. Proc. Natl. Acad. Sci. U. S. A. 104, 5163–8. doi:10.1073/pnas.0700293104

Barlow, H., 1961. Possible principles underlying the transformations of sensory messages. Sens. Commun. doi:10.7551/mitpress/9780262518420.003.0013

Barlow, H.B., 1953. Summation and inhibition in the frog's retina. J. Physiol. 119, 69–88. doi:10.1113/jphysiol.1953.sp004829

Bauer, J., Held, R., 1975. Comparison of visually guided reaching in normal and deprived infant monkeys. J. Exp. Psychol. Anim. Behav. Process. 1, 298–308.

Chen, T.-W., Wardill, T.J., Sun, Y., Pulver, S.R., Renninger, S.L., Baohan, A., Schreiter, E.R., Kerr, R. a, Orger, M.B., Jayaraman, V., Looger, L.L., Svoboda, K., Kim, D.S., 2013. Ultrasensitive fluorescent proteins for imaging neuronal activity. Nature 499, 295–300. doi:10.1038/nature12354

Clark, A., 2013. Whatever next? Predictive brains, situated agents, and the future of cognitive science. Behav. Brain Sci. 36, 181–204. doi:10.1017/S0140525X12000477

Dombeck, D.A., Khabbaz, A.N., Collman, F., Adelman, T.L., Tank, D.W., 2007. Imaging large-scale neural activity with cellular resolution in awake, mobile mice. Neuron 56, 43–57. doi:10.1016/j.neuron.2007.08.003

Fino, E., Yuste, R., 2011. Dense Inhibitory Connectivity in Neocortex. Neuron 69, 1188–1203. doi:10.1016/j.neuron.2011.02.025

Friston, K., 2010. The free-energy principle: a unified brain theory? Nat. Rev. Neurosci. 11, 127–38. doi:10.1038/nrn2787

Friston, K., Kiebel, S., 2009. Predictive coding under the free-energy principle. Philos. Trans. R. Soc. Lond. B. Biol. Sci. 364, 1211–21. doi:10.1098/rstb.2008.0300

Frith, C.D., Blakemore, S., Wolpert, D.M., 2000. Explaining the symptoms of schizophrenia: abnormalities in the awareness of action. Brain Res. Brain Res. Rev. 31, 357–63.

Fu, Y., Tucciarone, J.M., Espinosa, J.S., Sheng, N., Darcy, D.P., Nicoll, R.A., Huang, Z.J., Stryker, M.P., 2014. A cortical circuit for gain control by behavioral state. Cell 156, 1139–52. doi:10.1016/j.cell.2014.01.050

Gerfen, C.R., Paletzki, R., Heintz, N., 2013. GENSAT BAC Cre-Recombinase Driver Lines to Study the Functional Organization of Cerebral Cortical and Basal Ganglia Circuits. Neuron 80, 1368–1383. doi:10.1016/j.neuron.2013.10.016

Gong, S., Doughty, M., Harbaugh, C.R., Cummins, A., Hatten, M.E., Heintz, N., Gerfen, C.R., 2007.

Targeting Cre recombinase to specific neuron populations with bacterial artificial chromosome constructs. J. Neurosci. 27, 9817–23. doi:10.1523/JNEUROSCI.2707-07.2007

Han, X., Chow, B.Y., Zhou, H., Klapoetke, N.C., Chuong, A., Rajimehr, R., Yang, A., Baratta, M. V, Winkle, J., Desimone, R., Boyden, E.S., 2011. A high-light sensitivity optical neural silencer: development and application to optogenetic control of non-human primate cortex. Front. Syst. Neurosci. 5, 18. doi:10.3389/fnsys.2011.00018

Hartline, H.K., 1938. The response of single optic nerve fibers of the vertebrate eye to illumination of the retina. Am. J. Physiol. -- Leg. Content 121.

Heiman, M., Schaefer, A., Gong, S., Peterson, J.D., Day, M., Ramsey, K.E., Suárez-Fariñas, M., Schwarz, C., Stephan, D. a, Surmeier, D.J., Greengard, P., Heintz, N., 2008. A translational profiling approach for the molecular characterization of CNS cell types. Cell 135, 738–48. doi:10.1016/j.cell.2008.10.028

Hein, A., Held, R., 1967. Dissociation of the visual placing response into elicited and guided components. Science 158, 390–2.

Hein, a, Held, R., Gower, E.C., 1970. Development and segmentation of visually controlled movement by selective exposure during rearing. J. Comp. Physiol. Psychol. 73, 181–7.

Held, R., Bossom, J., 1961. Neonatal deprivation and adult rearrangement: complementary techniques for analyzing plastic sensory-motor coordinations. J. Comp. Physiol. Psychol. 54, 33–7.

Held, R., Freedman, S.J., 1963. Plasticity in human sensorimotor control. Science 142, 455–62.

Held, R., Hein, A., 1963. Movement-produced stimulation in the development of visually guided behavior. J. Comp. Physiol. Psychol. 56, 872–6.

Hippenmeyer, S., Vrieseling, E., Sigrist, M., Portmann, T., Laengle, C., Ladle, D.R., Arber, S., 2005. A developmental switch in the response of DRG neurons to ETS transcription factor signaling. PLoS Biol. 3, e159. doi:10.1371/journal.pbio.0030159

Hubel, D.H., Wiesel, T.N., 1962. Receptive fields, binocular interaction and functional architecture in the cat's visual cortex. J. Physiol. 160, 106–54.

Hubel, D.H., Wiesel, T.N., 1959. Receptive fields of single neurones in the cat's striate cortex. J. Physiol. 148, 574–91.

Jiang, X., Shen, S., Cadwell, C.R., Berens, P., Sinz, F., Ecker, A.S., Patel, S., Tolias, A.S., 2015. Principles of connectivity among morphologically defined cell types in adult neocortex. Science 350, aac9462. doi:10.1126/science.aac9462

Keller, G.B., Bonhoeffer, T., Hübener, M., 2012. Sensorimotor mismatch signals in primary visual cortex of the behaving mouse. Neuron 74, 809–15. doi:10.1016/j.neuron.2012.03.040

Klapoetke, N.C., Murata, Y., Kim, S.S., Pulver, S.R., Birdsey-Benson, A., Cho, Y.K., Morimoto, T.K., Chuong, A.S., Carpenter, E.J., Tian, Z., Wang, J., Xie, Y., Yan, Z., Zhang, Y., Chow, B.Y., Surek, B., Melkonian, M., Jayaraman, V., Constantine-Paton, M., Wong, G.K.-S., Boyden, E.S., 2014. Independent optical excitation of distinct neural populations. Nat. Methods 11, 338–346. doi:10.1038/nmeth.2836

Leinweber, M., Zmarz, P., Buchmann, P., Argast, P., Hübener, M., Bonhoeffer, T., Keller, G.B., 2014. Two-photon calcium imaging in mice navigating a virtual reality environment. J. Vis. Exp. e50885. doi:10.3791/50885

Madisen, L., Zwingman, T.A., Sunkin, S.M., Oh, S.W., Zariwala, H.A., Gu, H., Ng, L.L., Palmiter, R.D., Hawrylycz, M.J., Jones, A.R., Lein, E.S., Zeng, H., 2010. A robust and high-throughput Cre reporting and characterization system for the whole mouse brain. Nat. Neurosci. 13, 133–40. doi:10.1038/nn.2467

Markram, H., Toledo-Rodriguez, M., Wang, Y., Gupta, A., Silberberg, G., Wu, C., 2004. Interneurons of the neocortical inhibitory system. Nat. Rev. Neurosci. 5, 793–807. doi:10.1038/nrn1519

Marr, D., 2010. Vision. The MIT Press. doi:10.7551/mitpress/9780262514620.001.0001

Miller, M.W., Vogt, B.A., 1984. Direct connections of rat visual cortex with sensory, motor, and association cortices. J. Comp. Neurol. 226, 184–202. doi:10.1002/cne.902260204

Niell, C.M., Stryker, M.P., 2010. Modulation of visual responses by behavioral state in mouse visual cortex. Neuron 65, 472–9. doi:10.1016/j.neuron.2010.01.033

Pfeffer, C.K., Xue, M., He, M., Huang, Z.J., Scanziani, M., 2013. Inhibition of inhibition in visual cortex: the logic of connections between molecularly distinct interneurons. Nat. Neurosci. 16, 1068–76. doi:10.1038/nn.3446

Pi, H.-J., Hangya, B., Kvitsiani, D., Sanders, J.I., Huang, Z.J., Kepecs, A., 2013. Cortical interneurons that specialize in disinhibitory control. Nature 503, 521–4. doi:10.1038/nature12676

Rao, R.P., Ballard, D.H., 1999. Predictive coding in the visual cortex: a functional interpretation of some extra-classical receptive-field effects. Nat. Neurosci. 2, 79–87. doi:10.1038/4580

Riesen, A.H., Aarons, L., 1959. Visual movement and intensity discrimination in cats after early deprivation of pattern vision. J. Comp. Physiol. Psychol. 52, 142–9.

Saleem, A.B., Ayaz, A., Jeffery, K.J., Harris, K.D., Carandini, M., 2013. Integration of visual motion and locomotion in mouse visual cortex. Nat. Neurosci. doi:10.1038/nn.3567

Sherrington, C.S., 1906. Observations on the scratch-reflex in the spinal dog. J. Physiol. 34, 1–50. doi:10.1113/jphysiol.1906.sp001139

Sinha, P., Kjelgaard, M.M., Gandhi, T.K., Tsourides, K., Cardinaux, A.L., Pantazis, D., Diamond, S.P., Held, R.M., 2014. Autism as a disorder of prediction. Proc. Natl. Acad. Sci. U. S. A. doi:10.1073/pnas.1416797111

Spillmann, L., 2014. Receptive fields of visual neurons: the early years. Perception 43, 1145–76.

Spratling, M.W., 2008. Predictive coding as a model of biased competition in visual attention. Vision Res. 48, 1391–408. doi:10.1016/j.visres.2008.03.009

Taniguchi, H., He, M., Wu, P., Kim, S., Paik, R., Sugino, K., Kvitsiani, D., Kvitsani, D., Fu, Y., Lu, J., Lin, Y., Miyoshi, G., Shima, Y., Fishell, G., Nelson, S.B., Huang, Z.J., 2011. A resource of Cre driver lines for genetic targeting of GABAergic neurons in cerebral cortex. Neuron 71, 995–1013. doi:10.1016/j.neuron.2011.07.026

Vogt, B.A., Miller, M.W., 1983. Cortical connections between rat cingulate cortex and visual, motor, and postsubicular cortices. J. Comp. Neurol. 216, 192–210. doi:10.1002/cne.902160207

Vong, L., Ye, C., Yang, Z., Choi, B., Chua, S., Lowell, B.B., 2011. Leptin action on GABAergic neurons prevents obesity and reduces inhibitory tone to POMC neurons. Neuron 71, 142–54. doi:10.1016/j.neuron.2011.05.028

Wilson, N.R., Runyan, C. a, Wang, F.L., Sur, M., 2012. Division and subtraction by distinct cortical inhibitory networks in vivo. Nature 488, 343–8. doi:10.1038/nature11347

Xue, M., Atallah, B. V., Scanziani, M., 2014. Equalizing excitation–inhibition ratios across visual cortical neurons. Nature. doi:10.1038/nature13321

Zhang, S., Xu, M., Kamigaki, T., Hoang Do, J.P., Chang, W.-C., Jenvay, S., Miyamichi, K., Luo, L., Dan, Y., 2014. Long-range and local circuits for top-down modulation of visual cortex processing. Science (80-.). 345, 660–665. doi:10.1126/science.1254126

Zmarz, P., Keller, G.B., 2016. Mismatch Receptive Fields in Mouse Visual Cortex. Neuron 92, 766–772. doi:10.1016/j.neuron.2016.09.057